



# AMERICAN METEOROLOGICAL SOCIETY

*Bulletin of the American Meteorological Society*

## **EARLY ONLINE RELEASE**

This is a preliminary PDF of the author-produced manuscript that has been peer-reviewed and accepted for publication. Since it is being posted so soon after acceptance, it has not yet been copyedited, formatted, or processed by AMS Publications. This preliminary version of the manuscript may be downloaded, distributed, and cited, but please be aware that there will be visual differences and possibly some content differences between this version and the final published version.

The DOI for this manuscript is doi: 10.1175/BAMS-D-15-00320.1

The final published version of this manuscript will replace the preliminary version at the above DOI once it is available.

If you would like to cite this EOR in a separate work, please use the following full citation:

Roberts, M., P. Vidale, C. Senior, H. Hewitt, C. Bates, S. Berthou, P. Chang, H. Christensen, S. Danilov, M. Demory, S. Griffies, R. Haarsma, T. Jung, G. Martin, S. Minobe, T. Ringler, M. Satoh, R. Schiemann, E. Scoccimarro, G. Stephens, and M. Wehner, 2018: The benefits of global high-resolution for climate simulation: process-understanding and the enabling of stakeholder decisions at the regional scale. Bull. Amer. Meteor. Soc. doi:10.1175/BAMS-D-15-00320.1, in press.



# The benefits of global high-resolution for climate simulation: process-understanding and the enabling of stakeholder decisions at the regional scale.

M. J. Roberts<sup>1\*</sup>, P. L. Vidale<sup>2</sup>, C. Senior<sup>1</sup>, H.T. Hewitt<sup>1</sup>, C. Bates<sup>3</sup>, S. Berthou<sup>1</sup>, P. Chang<sup>4</sup>, H. M. Christensen<sup>5</sup>, S. Danilov<sup>6</sup>, M.-E. Demory<sup>2,16</sup>, S. M. Griffies<sup>7</sup>, R. Haarsma<sup>8</sup>, T. Jung<sup>6,9</sup>, G. Martin<sup>1</sup>, S. Minobe<sup>10</sup>, T. Ringler<sup>11</sup>, M. Satoh<sup>12</sup>, R. Schiemann<sup>2</sup>, E. Scoccimarro<sup>13</sup>, G. Stephens<sup>14,1,2</sup>, M. F. Wehner<sup>15</sup>

<sup>1</sup> Met Office, Fitzroy Road, Exeter. EX1 3PB, UK

<sup>2</sup> National Centre for Atmospheric Science, University of Reading, Reading, UK

<sup>3</sup> University of Exeter, Exeter, UK

<sup>4</sup> Department of Oceanography, Texas A&M University, Texas, USA

<sup>5</sup> Atmospheric, Oceanic and Planetary Physics, University of Oxford, Oxford, UK

<sup>6</sup> Alfred Wegener Institute, Helmholtz Centre for Polar and Marine Research, Bremerhaven, Germany

<sup>7</sup> NOAA/GFDL, Princeton, NJ, USA

<sup>8</sup> Royal Netherlands Meteorological Institute, De Bilt, The Netherlands

<sup>9</sup> Department of Physics and Electrical Engineering, University of Bremen, Bremen, Germany

<sup>10</sup> Division of Earth and Planetary Sciences, Faculty of Science, Hokkaido University, Sapporo, Japan

<sup>11</sup> Theoretical Division, Los Alamos National Laboratory, Los Alamos, NM, USA

<sup>12</sup> Atmosphere and Ocean Research Institute, The University of Tokyo, Tokyo, Japan

<sup>13</sup> Fondazione Centro euro-Mediterraneo sui Cambiamenti Climatici (CMCC), Bologna, Italy

<sup>14</sup> Jet Propulsion laboratory, California Institute of Technology, Pasadena, California, USA

<sup>15</sup> Computational Research Division, Lawrence Berkeley National Laboratory, Berkeley, California, USA

<sup>16</sup> Center for Space and Habitability, University of Bern, Bern, Switzerland

\*Corresponding author address: Malcolm J. Roberts, Met Office Hadley Centre, FitzRoy Road, Exeter EX1 3PB, United Kingdom.

Email: malcolm.roberts@metoffice.gov.uk

For: *Bulletin of the American Meteorological Society*

Capsule summary:

A perspective on current and future capabilities in global high-resolution climate simulation for assessing climate risks over next few decades, including advances in process representation and analysis, justifying the emergence of dedicated, coordinated experimental protocols.

## Abstract

1  
2  
3  
4  
5  
6  
7  
8  
9  
10  
11  
12  
13  
14  
15  
16  
17  
18  
19  
20  
21  
22  
23  
24  
25  
26  
27  
28  
29  
30  
31  
32

The timescales of the Paris Climate Agreement indicate urgent action is required on climate policies over the next few decades, in order to avoid the worst risks posed by climate change. On these relatively short timescales the combined effect of climate variability and change are both key drivers of extreme events, with decadal timescales also important for infrastructure planning. Hence, in order to assess climate risk on such timescales, we require climate models to be able to represent key aspects of both internally driven climate variability, as well as the response to changing forcings.

In this paper we argue that we now have the modelling capability to address these requirements - specifically with global models having horizontal resolutions considerably enhanced from those typically used in previous IPCC and CMIP exercises. The improved representation of weather and climate processes in such models underpins our enhanced confidence in predictions and projections, as well as providing improved forcing to regional models, which are better able to represent local-scale extremes (such as convective precipitation). We choose the global water cycle as an illustrative example, because it is governed by a chain of processes for which there is growing evidence of the benefits of higher resolution. At the same time it comprises key processes involved in many of the expected future climate extremes (e.g. flooding, drought, tropical and mid-latitude storms).

### 33 Introduction

34

35 Our capability to perform global climate model simulations suitable to inform  
36 societal action is constrained by both available computer resources and the  
37 efficiency of the algorithms used in our models. Multi-exaflop computer power  
38 would be needed for global climate models to produce multi-member ensemble,  
39 multi-century simulations at resolutions capable of resolving macroscopic cloud  
40 features and ocean mesoscale eddies. Estimates suggest that such computer  
41 power is at least a decade away. Yet, given the enormous scale of  
42 supercomputing about to be used for the next Coupled Model Intercomparison  
43 Project (CMIP6; Eyring et al. 2016), we feel that this is a particularly important  
44 time to review our current status in present-day high-resolution global climate  
45 modeling.

46

47 At one extreme, numerous climate model simulations are performed as part of  
48 each CMIP cycle (Meehl et al. 2000; Meehl et al. 2007; Taylor et al. 2012;  
49 Eyring et al. 2016), organized by the World Climate Research Programme  
50 (WCRP). Such models typically include aspects of Earth System complexity  
51 such as biogeochemistry, and simulations including several ensemble  
52 members are usually completed. However, in order to achieve this task, the  
53 horizontal resolution has traditionally been compromised, typically to ~150km  
54 or coarser in the atmosphere and 1 degree in the ocean. This means that  
55 important climate processes (such as atmospheric convection, ocean  
56 mesoscale boundary currents and eddies) have had to be parameterised rather  
57 than resolved, and dynamical processes and interactions can be compromised  
58 (Collins et al. 2018).

59

60 At the opposite extreme, the next major breakthrough in simulation may be  
61 reached at scales below 1 km in the atmosphere, as we come close to resolving  
62 the largest of boundary-layer eddies, the macroscopic cloud features and  
63 convective organisation (Schneider et al. 2017). Several global models (e.g.  
64 NICAM; Satoh et al. 2008, 2014) are now able to complete global simulations  
65 at sub-km grid spacing (Miyamoto et al. 2014). Such individual simulations are

66 currently short (<1 year), have only a minimal number of Earth System  
67 processes included, and challenge our observational abilities, due to the limited  
68 time and space sampling from satellites. However, they can be used to gain  
69 insights into poorly understood interactions (such as aerosol-microphysics-  
70 cloud interactions, e.g. Hashino et al. 2013). Such models are also generally  
71 non-hydrostatic and hence able to better represent organised convective  
72 processes and small-scale structures in, for example, tropical cyclones.  
73 Considerable uncertainties remain, but such tools are key for future process  
74 understanding.

75

76 In between these two fundamental scale boundaries, gradual refinements in  
77 resolution might be considered to afford only marginal benefits for our  
78 understanding of climate variability and change. However, here we aim to  
79 demonstrate that significant improvements in understanding are afforded by  
80 global models at intermediate resolutions, which are vital for projections over  
81 the next few decades. We show evidence that the large-scale circulation is  
82 significantly improved in the atmosphere using resolutions finer than 100km,  
83 despite the Rossby radius being ~1000km and hence “resolved” in CMIP-type  
84 models. For the ocean, the Rossby radius is finer than 100km and hence  
85 unresolved in most CMIP-ocean models, with potentially important  
86 consequences for climate simulation (Hewitt et al. 2017).

87

88 Global NWP models have paved the way for developments in climate modelling  
89 and systematically demonstrated the added benefits of enhanced resolution,  
90 albeit in the context of initialised forecasts, which also benefit from advances in  
91 other components (such as data assimilation, ensemble size, number of  
92 observations and other model improvements; Magnusson and Källén, 2013;  
93 Bauer et al, 2015). With the advent of seamless modelling approaches (e.g.  
94 Senior et al. 2009; Brown et al. 2012), NWP and climate models are becoming  
95 equivalent in their scientific configurations, and many biases seen in long term  
96 climate simulations are already evident after days of an NWP forecast (Martin  
97 et al. 2010). An example of monitoring progress in NWP, citing resolution as  
98 one aspect of improvements in skills scores, is shown in Fig. 10 of Rodwell et

99 al. (2010). A more general, high-level review of the benefits of resolution in  
100 NWP models is provided by Wedi (2014).

101

102 Hence some of the following evidence from climate models is far from unique  
103 to them. However, aspects of the hydrological cycle have typically not been a  
104 part of NWP skill assessments (which, for example, usually concentrate on  
105 large-scale quantities that are relevant to users on short-range timescales, such  
106 as 500 hPa height, 250 hPa winds and temperature; see references above and  
107 Mittermaier et al. 2016). In addition, and more crucially, the NWP modelling  
108 systems are typically neither radiatively balanced nor water-conserving, so are  
109 not well-placed for systematic process studies of water cycle processes on  
110 longer time- and space-scales.

111

112 Regional models are increasingly being used for climate studies at resolutions  
113 of several kilometres (Kendon et al. 2017). One could argue that this approach  
114 mitigates the need for refinements to global model resolutions. Indeed if the  
115 requirement is to understand local processes (such as convective precipitation)  
116 and extremes in terms of their local impacts, then such models currently  
117 represent our best tools. However, the regional models' representation of the  
118 large-scale circulation is no better than that of the driving global model  
119 (otherwise it would not be well constrained), and this requires the global model  
120 to credibly represent global modes of variability, dynamic and thermodynamic  
121 responses to climate forcing. Hence it is key to make the large-scale circulation  
122 as accurate as possible, as this provides critical information needed for the  
123 regional downscaling to offer added information. We will argue that it is  
124 precisely at these synoptic scales that the new generation of high-resolution  
125 global models are showing substantial improvement in the mean state and  
126 variability.

127

128 We ask in this paper what we can learn from the range of models at global  
129 resolutions that are now or will soon become affordable on flagship  
130 supercomputers worldwide. In particular we ask what added value such  
131 enhanced models provide in terms of the simulated hydrological cycle, and thus

132 the trustworthiness and robustness of current climate projections particularly  
133 over the next few decades.

134

### 135 [The global hydrological cycle](#)

136

137 One of the key questions for climate research is how the global water cycle  
138 might change in the next few decades. At its most basic, the global water cycle  
139 describes the movement of water between the different reservoirs in the climate  
140 system - in and on the ocean (including sea-ice and ice shelves), over and  
141 below the land surface (surface and ground water, land-ice), and the  
142 corresponding energy exchanges. It is therefore implicated in many of the  
143 impacts that climate change brings - excess water (flooding, tropical and mid-  
144 latitude storms, atmospheric rivers), lack of water (drought), and intensity of  
145 storms (concurrently regulated by energy and momentum exchanges).

146

147 The representation of the global water cycle in coupled climate models, and in  
148 particular some of its governing processes, is subject to much larger variability  
149 among models than other (thermodynamic) indicators. One can contrast the  
150 significant agreement in CMIP5 (Flato et al. 2013), expressed by model  
151 projections of future warming rates and patterns, against the disagreement in  
152 projected precipitation changes, which showed little improvement over the  
153 earlier CMIP3 assessment. Although precipitation does not represent the whole  
154 water cycle, and our observational record is short and uncertain, such  
155 fundamental disagreements do not build confidence in future projections.

156

157 Part of the reason for this uncertainty is the lack of representation of the  
158 dynamical aspects of the coupled climate system, and how these are coupled  
159 to the physical aspects of model simulation. At the largest scales, on the order  
160 of the Rossby radius, model physics (i.e. column processes) dominate the  
161 under-resolved dynamics in atmosphere and ocean (Trenberth et al. 2011;  
162 Demory et al. 2014). As resolution increases and the synoptic and mesoscales  
163 become better resolved, then they both play an important role – perhaps at a  
164 minimal resolution of around 50km (Matsueda and Palmer 2011; Delworth et  
165 al. 2012, Demory et al. 2014). As resolution increase continues towards the 1



166 km-scale, multi-scale dynamics increasingly dominates column physics (see for  
167 instance the discussion in Vellinga et al. 2016).

168

169 *a. Large-scale moisture transports*

170 Studies focusing on the impact of resolution on the simulated global  
171 hydrological cycle as a whole remain quite rare (Pope and Stratton 2002; Hack  
172 et al. 2006; Hagemann et al. 2006; Demory et al. 2014). Demory et al. (2014)  
173 find that the simulation of a select few components of the global hydrological  
174 cycle is degraded by increasing model resolution, due to an overall excess in  
175 net available energy at the surface that is caused by errors in model physics.  
176 However, they find that the overall hydrological cycle is intensified by global  
177 grid refinement, and for consistent reasons, resulting in a strength that  
178 compares well with observations (e.g. as in Trenberth et al. 2011). This is  
179 manifested by less precipitation over the ocean and more precipitation over  
180 land, caused by enhanced large-scale atmospheric moisture transport from the  
181 ocean to the land, reducing the commonly overestimated precipitation recycling  
182 over land. At mid-latitudes, this increase in the large-scale atmospheric  
183 moisture transport is particularly associated with the storm track regions.  
184 Notably, such multi-scale interactions can only be studied with global models.  
185 Demory et al. (2014) also uncovered a locally asymptotic response of the mid-  
186 latitude large-scale atmospheric moisture transport, starting at about 60 km grid  
187 size, which seems to be within recent observational estimates (Trenberth et al.  
188 2011). There are indications that other models show similar sensitivity to  
189 resolution (Terai et al. 2017; Vanniere et al., submitted).

190

191 *b. Surface water balance and precipitation distribution*

192 Precipitation, evaporation, runoff and storage variations characterise the water  
193 balance over any land area. All four of these quantities are difficult to observe  
194 and to simulate by global climate models, and our current ability to close the  
195 water balance remains highly unsatisfactory over the global land area and much  
196 more so at the scales of continents or large river basins. One example of these  
197 uncertainties is illustrated in Figure 1: total global precipitation is remarkably  
198 resolution invariant, which points to a very robust constraint provided by global  
199 long-wave cooling in all model simulations, producing precipitation estimates

200 within the range of significant and persistent observational uncertainty (see  
201 estimates by GPCP versus Wild et al. 2015 versus Stephens et al. 2012).  
202 Further, increasing the resolution in the HadGEM3 atmospheric GCM (GA3,  
203 Mizieliński et al 2014) from about 100 to 25 km changes the model estimate of  
204 precipitation partitioning. Land versus sea distribution of precipitation agrees  
205 with the findings in Demory et al. 2014; additionally, for the land portion, global  
206 (rugged) mountain precipitation increases by about 15%, and available  
207 observations, which are sparse over complex terrain, are hardly able to assess  
208 these model estimates. Precipitation over comparatively small mountain areas  
209 is particularly important since it disproportionately contributes to runoff and  
210 therefore the generation of so-called blue water which sustains ecosystems and  
211 human livelihood.

212

213 Given such uncertainties in global precipitation, it is not surprising that regional  
214 distributions are also poorly estimated. Figure 2, reproduced from Wehner et  
215 al. (2014), shows an analysis of annual daily total precipitation distributions from  
216 three different horizontal resolutions of the Community Atmospheric Model  
217 (CAM5.1), for a number of regions. There is some evidence that, at resolutions  
218 finer than 25km, grid separation is no longer the limiting factor in reproducing  
219 observations (e.g. Hawcroft et al. 2016) and that deficiencies in sub-grid scale  
220 parameterisations dominate the model errors (Wehner et al. 2014), particularly  
221 when convection is an important contributor to the local atmospheric water  
222 budget.

223

224 Using the same ensemble of GA3 atmospheric model simulations as Demory  
225 et al. (2014) at 130km, 60km and 25km resolution (referred to as N96, N216  
226 and N512 respectively), the precipitation distribution in each IPCC SREX<sup>1</sup>  
227 region is used to determine which model resolution best fits the multiple  
228 observational datasets available over that region (see Appendix A for details).  
229 Figure 3 shows the coarsest best resolution for each region. Several key points  
230 become evident:

---

<sup>1</sup> Special Report on Managing the Risks of Extreme Events and Disasters to Advance Climate Change Adaptation

- 231 1. In most regions a resolution finer than 130km is worthwhile;
- 232 2. Globally 60km may be sufficient for this metric, but there are some
- 233 regions (e.g. Western Africa, South Eastern Asia) which consistently favour
- 234 25km resolution, often where land-sea contrasts and/or mountainous terrain
- 235 exist; note also that at latitudes polewards of 50°, the only long-term global
- 236 observational datasets have resolutions of 110km and hence it not possible to
- 237 properly assess higher resolution models;
- 238 3. There are some regions which are uncertain, either because no model
- 239 is clearly better or the observational datasets disagree too much with each other
- 240 to assign a best model resolution (i.e. we do not know the climatology well
- 241 enough to validate models).

242

### 243 *c. Dynamical processes and moisture transport*

244 Correct attribution of the processes responsible for the global distribution of

245 precipitation is key, because models that produce a reasonable climatology via

246 demonstrably incorrect processes cannot be trusted for climate projections of

247 rainfall.

248

### 249 *Extra-Tropical Cyclones*

250 One likely component driving the sensitivity of simulated moisture transport and

251 precipitation to resolution is the moisture transport effected by dynamical

252 processes such as cyclones (both tropical and mid-latitude). Storms provide a

253 considerable proportion of annual rainfall in many regions of the world

254 (Scoccimarro et al 2014; Guo et al 2017), and as such representing their

255 frequency, variability, position and composition is important. Catto et al. (2010)

256 and Zappa et al. (2013) show that extratropical storm structure and intensity

257 are better represented at resolutions finer than 100km, and hence the moisture

258 transport associated with them. Jung et al. (2012) demonstrate significantly

259 improved extratropical cyclone frequency when moving from 130km to 40km

260 resolution, with little change at finer grid spacings.

261

### 262 *Tropical Cyclones and African Easterly Waves*

263 There is mounting evidence from many modelling studies that atmosphere

264 resolutions at 50km or finer skilfully represent the interannual variability of

265 tropical cyclones (Zhao et al, 2009; Manganello et al. 2012; Roberts et al, 2014;  
266 Kodama et al. 2015). In the Atlantic, much of this improvement can be attributed  
267 to better global teleconnections (from El Niño, for example, Bell et al. 2014)  
268 providing a constraint on the environment, and improved dynamical precursor  
269 features such as African Easterly Waves (AEWs). Despite the latter being  
270 relatively large-scale dynamical systems, they are poorly represented at ~100  
271 km grid scales (Martin and Thorncroft, 2015; Caron et al, 2011). This re-  
272 emphasises the danger of assuming that representation by at least two grid  
273 points is sufficient for resolving features.

274

275 Tropical cyclone importance is not only limited to producing high-impact events:  
276 Guo et al. (2017) showed that typhoons in East Asia produce about 50% of  
277 precipitation in coastal areas at the peak of the season, but also contribute a  
278 sizeable portion of the moisture transport that supports all other types of  
279 precipitation further inland. Further, their net contribution to the regional  
280 moisture budget of China is comparable albeit opposite to that of the monsoon  
281 at the time of its recession. Scoccimarro et al. (2014) show a similar result for  
282 the North Atlantic tropical cyclones and US precipitation, while Pantillon et al.  
283 (2015) show a remote link to Mediterranean rainfall events. These impacts  
284 require fidelity in storm characteristics, with Figure 4 (from Manganello et al.  
285 2014) illustrating the improvement of storm genesis and track as model  
286 resolution is enhanced, while Scoccimarro et al. (2017) demonstrated the  
287 additional importance of high frequency coupling between atmosphere and  
288 ocean.

289

### 290 *Mesoscale Convective Systems*

291 In addition to storms influencing the mean precipitation, Vellinga et al. (2014)  
292 have shown important scale interactions between large-scale variability and  
293 smaller scales. Decadal variability in Sahel rainfall is shown to be related to the  
294 interaction between the large-scale Atlantic Multi-Decadal Oscillation (AMO)  
295 and AEWs. Only model resolutions fine enough (at 60km and finer in that study)  
296 to represent stronger, self-organised (at the mesoscale) and propagating  
297 rainfall events capture the observed decadal trends. There are indications that  
298 other CMIP5 models follow this relationship, but analysis is complicated by

299 confounding factors such as different aerosol loadings, indicating a need for a  
300 more systematic set of comparable simulations.

301

### 302 *Westerly Wind Bursts*

303 Aforementioned dynamical precursor systems such as AEWs are also found to  
304 be important in driving variability in other dynamical systems. If they are poorly  
305 represented in models, this can significantly bias the simulated mean state, and  
306 hence lead to misleading future projections. One example would be the  
307 westerly wind bursts (WWBs) in the tropical Pacific that precede El Niño events:  
308 in observations the irregular variability of ENSO has been attributed to such  
309 WWB events (Puy et al. 2017). It may be possible that the inclusion of  
310 stochastic schemes (Christensen et al. 2017) enables some of the aspects of  
311 these precursor systems to be replicated. However development of such  
312 stochastic schemes is best informed by models able to simulate the dynamical  
313 aspects of these processes, as well as the physics-dynamics coupling.

314

### 315 *Monsoons*

316 In the tropics, the monsoon circulations provide a large portion of annual rainfall  
317 to many regions. There are many components and individual processes within  
318 these circulations (flow reversals, orographic interactions, land-sea contrasts,  
319 sensitivity to remote biases), and this may be why increased model resolution  
320 does not directly lead to improved monsoon simulation (Ogata et al. 2017;  
321 Johnson et al. 2016). Individual components do indicate a resolution sensitivity  
322 (such as monsoon depressions, Johnson et al. 2016), but reduction of remote  
323 biases to improve the regional mean state may be equally important (Levine  
324 and Martin 2017; Martin et al. 2010).

325

### 326 *Atmospheric Blocking*

327 At mid-latitudes, the representation of storm tracks and blocking play important  
328 roles in the large-scale dynamics of the water cycle. Dawson et al. (2012)  
329 demonstrate a large improvement in the structure of Euro-Atlantic weather  
330 regimes in a model run at 16km compared to one run at 150km, while Dawson  
331 and Palmer (2015) show a 40km simulation has intermediate regime fidelity.  
332 The distribution, frequency and development of European blocking has been

333 shown to be influenced by aspects of atmosphere and ocean resolution  
334 (Berckmans et al 2013). Schiemann et al. (2017) showed some improvement  
335 in blocking in a multi-model atmosphere ensemble at 25km compared to  
336 ~100km, consistent with Jung et al. (2012) results when moving from 130km to  
337 40km. Scaife et al. (2011) showed how reducing large-scale model biases in  
338 the North Atlantic with a 1/4 degree ocean resolution led to improved frequency  
339 of European blocking. O'Reilly et al. (2016) studied blocking and extended cold  
340 spells over Europe, and showed that the resolution of remote SST fronts was a  
341 key factor in reinforcing the blocking anticyclone and hence extending the  
342 timescale of the events.

343

#### 344 *Ocean dynamics*

345 The impact of resolution on dynamical processes affecting the hydrological  
346 cycle is not limited to the atmosphere. In particular, the transport of freshwater  
347 is related to the stability of the meridional overturning circulation (Drifhout et al.  
348 2013). Since transport of freshwater can take place in narrow currents and  
349 eddies, this points to an important role for ocean resolution. In the South  
350 Atlantic, the transport of freshwater is strongly determined by Agulhas eddies  
351 which move salt from the Indian Ocean to the Atlantic Ocean (Drifhout et al.  
352 2003). In this region, resolution is key to the simulation of the Agulhas  
353 retroflexion and the shedding of eddies (Banks et al. 2007; Biastoch et al.  
354 2008). In the North Atlantic, ocean resolution is important for capturing the East  
355 Greenland current which transports freshwater from both sea ice melt and  
356 potential ice sheet melt into the Atlantic (Böning et al., 2016).

357

#### 358 *d. Land-Atmosphere coupling strength*

359 The asymptotic behavior with resolution uncovered by Demory et al. (2014) and  
360 discussed earlier is directly relevant to the correct representation of land-  
361 atmosphere coupling in GCMs: at scales finer than 50km, the systematic  
362 overestimation of the contribution of land evaporation to precipitation starts to  
363 be mitigated by realistic simulation of atmospheric moisture convergence.  
364 However, observational evidence indicates that we must also simulate  
365 mesoscale circulations generated by landscape heterogeneity, at horizontal  
366 scales of 10km or less. For instance, Taylor (2012) showed that precipitation

367 over the Sahel occurs over dry land patches, but coarse GCMs preferentially  
368 produce precipitation over moist patches, where convective parameterisation  
369 responds to surface moist static energy. This is because they do not represent  
370 the mesoscale horizontal transports of moisture between different land patches.  
371 The phase of the diurnal cycle of precipitation over land can also impact land-  
372 atmosphere coupling, and is almost uniformly poorly simulated in GCMs (Slingo  
373 et al. 1992; Bechtold et al. 2004; Clark et al. 2007; Ackerley et al. 2015) with  
374 implications for surface energy and moisture budgets. Recent convective  
375 parameterisations (e.g. Bechtold et al. 2014) have improved the diurnal cycle  
376 phase, while Birch et al. (2015) demonstrated similar capability by disabling  
377 convective parameterisation at around 10km resolution.

378

379 *e. Air-sea interactions*

380 The ocean's mesoscale influence on the atmosphere in the extra tropics has  
381 been known from observational analyses for some time, both near-surface  
382 (e.g., Chelton et al. 2004; Xie 2004) and in the free troposphere via  
383 precipitation, clouds and upward winds (e.g., Minobe et al. 2008; 2010;  
384 Tokinaga et al. 2009; Frenger et al. 2013; Ma, J. et al. 2015, Smirnov et al.  
385 2015). However, it has required deployment of models with sufficient resolution  
386 in both the atmosphere and ocean in order to study and understand such  
387 interactions at the process level (Small et al. 2008; Chelton and Xie 2010, Kwon  
388 et al, 2010; Ma, J. et al.; 2015; Ma, X. et al. 2016).

389 Coupled simulations demonstrate fundamental changes in the character of  
390 atmosphere-ocean coupling once they admit the ocean mesoscale (Bryan et al.  
391 2010; Roberts et al 2016), with modelling confirming that SST forces the local  
392 winds at frontal- and mesoscales, as observed (Chelton et al. 2001). In contrast,  
393 when the ocean model uses a coarse grid (1.0° or coarser), the opposite is  
394 found (Kirtman et al. 2012). These results point to the high possibility that  
395 frontal- and mesoscale air-sea interactions are poorly represented in CMIP5  
396 models, consistent with the CMIP3 analysis by Maloney and Chelton (2006),  
397 with potential consequences for the fidelity of simulations of the hydrological  
398 cycle.

399

400 Atmospheric resolution is also important to capture coupled responses. For  
401 example, the salient feature of the Gulf Stream rain band (Minobe et al. 2008;  
402 2010) is captured by an atmospheric GCM of about 50km grid-spacing (Minobe  
403 et al. 2008; Kuwano-Yoshida et al. 2010; Scher et al. 2017). By direct  
404 comparisons between high-resolution and low-resolution regional atmospheric  
405 model simulations (Willison et al. 2013; Ma, X. et al. 2016; Hawcroft et al. 2017),  
406 it is shown that latent heat release associated with extratropical cyclone  
407 development is fundamentally important for realistic winter storm simulations,  
408 and it is only when the model has sufficient resolution to resolve small-scale  
409 diabatic heating that the full effect of mesoscale air-sea interactions on  
410 extratropical cyclogenesis can be correctly simulated.

411

412 The remote atmospheric response to oceanic fronts and eddies, in comparison  
413 to the local response, is generally more difficult to identify using direct  
414 observations (Frankignoul et al. 2011; O'Reilly and Czaja, 2015), hence most  
415 existing studies are based on high-resolution model experiments. A particularly  
416 useful experimental strategy for this type of study is a set of twin atmospheric  
417 model simulations, one of which is forced by observed SSTs and the other by  
418 spatially smoothed SSTs (Xie et al. 2002; Minobe et al. 2008; Kuwano-Yoshida  
419 et al. 2010; Small et al. 2014b; Piazza et al. 2015; Ma, X. et al. 2015 and 2016).  
420 These studies reveal how fine scale ocean features influence storm density  
421 (Minobe et al. 2008; Piazza et al. 2015), fronts (Masunaga et al. 2015; Parfitt et  
422 al. 2016); jet-stream shifts (Piazza et al. 2015; Ma, X. et al. 2015 and 2016;  
423 O'Reilly et al. 2017), storm-track strength (Small et al. 2014b) and remote  
424 rainfall response along US West Coast to Kuroshio eddies (Ma, X. et al. 2015  
425 and 2016; Kuwano-Yoshida and Minobe 2016).

426

#### 427 *f. Hydrological extremes*

428 Global models are useful for studying extremes in order to account for both  
429 teleconnected events and for events governed by the large-scale environment.  
430 For example the Russian heat wave of 2010 was part of the same wave train  
431 that led to the devastating Pakistan floods (Lau and Kim 2010; Watanabe et al.  
432 2010), while Atlantic tropical cyclones have been shown to affect Arctic sea ice  
433 cover (Scoccimarro et al. 2012). Assessing model skill in tropical cyclone



434 landfalling, where the large-scale steering flow is key, is in its infancy (e.g.  
435 Camp et al. 2015; Murakami et al. 2016), but this is clearly an important metric  
436 for impacts.

437

438 Despite improvements in simulation of tropical cyclones in CMIP5 (Walsh et al.  
439 2013), only a handful of global models showed any TCs reaching category 1  
440 hurricane/typhoon intensity. More recently the grid spacing in state of the art  
441 global models has become sufficiently fine (order of 10-30 km) to realistically  
442 represent TCs, even in terms of intensity (Manganello et al. 2012; Wehner et  
443 al. 2014; Wehner et al. 2015; Murakami et al. 2015; Walsh et al. 2015;  
444 Scoccimarro et al. 2016a; Scoccimarro et al. 2017), up to the maximum  
445 category 5. Our current understanding of future changes to frequency and  
446 intensity (Walsh et al. 2015) is based on these relatively few capable models,  
447 hence indicating a more systematic and multi-model study is required to  
448 increase our confidence in such interpretations.

449

450 The higher gradients of moisture and temperature simulated in high horizontal  
451 resolution global climate models are also important beyond the tropics, and  
452 projected to become more important in the future. The simulation of extra-  
453 tropical transition of tropical systems, and robust future projections thereof,  
454 show substantial sensitivity to resolution (Haarsma et al. 2013) thus  
455 representing new challenges and opportunities for the prediction of the  
456 changing risks posed by extreme precipitation, winds and storm surge  
457 impacting Europe.

458

### 459 [Future prospects and challenges](#)

460 There are an increasing number of modelling groups able to push our current  
461 modelling capability to the next level. This includes using km-scale global  
462 atmosphere and eddy-rich ocean simulations. Different methods are being tried  
463 to overcome the many associated technical challenges, ranging from more  
464 efficient algorithms to novel numerical methods. One factor that has so far been  
465 lacking is a large multi-model, multi-resolution ensemble of global simulations  
466 using a common experimental design to enable coordinated analysis. This is  
467 the goal of the CMIP6 HighResMIP project (Haarsma et al 2016), which

468 proposes a simple experimental design with the primary goal of assessing the  
469 robustness of projections across a multi-model ensemble, as a response to  
470 changes in the representation of climate processes with model horizontal  
471 resolution.

472

473 Using the CMIP6 HighResMIP protocol to create a multi-model reference  
474 dataset, work within the EU Horizon 2020 PRIMAVERA<sup>2</sup> project and with  
475 collaborators will also assess the costs and benefits of other advances:

476

477 1. Stochastic parameterisation schemes, which attempt to represent the  
478 variability of unresolved, sub-grid scale processes (Palmer 2009), offer a  
479 complementary approach to increasing model resolution. Due to nonlinearities  
480 in the system, including a zero-mean noise into a GCM leads to systematic  
481 shifts in the climate that can reduce model biases (Jung et al. 2005; Williams  
482 2012; Berner et al. 2015; 2017), and improve variability (Lin and Neelin 2000,  
483 2003; Dawson and Palmer 2015; Christensen et al 2015, 2017), often  
484 analogous to refining model resolution (e.g., Berner et al. 2012; Watson et al.  
485 2017)). As model resolution increases, stochastic approaches will become  
486 more valuable, as representing the interaction of the resolved scales with the  
487 sub-grid through purely deterministic schemes becomes harder to justify  
488 (Dorrestijn et al. 2013);

489

490 2. Global cloud-system resolving models are a particularly important tool for  
491 understanding multi-scale structures, such as the large-scale and synoptic  
492 environment of tropical cyclogenesis (Nakano et al. 2017; Yamada et al. 2017),  
493 or large-scale sea breezes and convection initiation (Birch et al. 2015). They  
494 also demonstrate the potential of models in complementing and enhancing  
495 observations, for example the discovery by Miyakawa et al. (2012) of the three-  
496 fold structure of convective momentum transport associated with MJO, using  
497 the high-resolution data by Miura et al. (2007);

498

---

<sup>2</sup> <https://www.primavera-h2020.eu>

499 3. Eddy-rich ocean models: the majority of CMIP5 climate projections were  
500 undertaken using coarse ( $1^\circ$  or coarser) ocean model components (typically  
501 with meridional refinement near the equator). At this grid spacing, the first  
502 baroclinic Rossby radius is resolved only near the equator (Hallberg, 2013).  
503 Hewitt et al. (2017) reviewed the improvements found in going towards eddy-  
504 poor/eddy-rich regimes ( $1/4^\circ - 1/10^\circ$ ), with important consequences for large-  
505 scale biases (McClellan et al. 2011; Delworth et al. 2012; Small et al. 2014a;  
506 Hewitt et al. 2016), heat uptake (e.g. Griffies et al. 2015; Kuhlbrodt et al. 2015)  
507 and ocean marine ecosystems (Saba et al. 2016; McKiver et al 2015; Stock et  
508 al. 2010). Coupled simulations with ocean resolutions up to  $1/16$  degree will  
509 enable investigation of the impact of eddies on the mean state and variability of  
510 the coupled system;

511

512 4. Unstructured meshes: an alternative approach to globally uniform increases  
513 in resolution is offered by a new generation of models for the atmosphere,  
514 ocean and sea ice, formulated on unstructured meshes (e.g., Danilov 2013;  
515 Ringler et al. 2013; Zarzycki et al., 2014; Sein et al. 2016). Unstructured  
516 meshes provide multi-resolution capacity, that is, they have the flexibility to  
517 enhance resolution where required. Several of the more mature unstructured  
518 mesh models (Finite Element Sea Ice-Ocean Model (FESOM), Wang et al.  
519 2008; Wang et al. 2014; Danilov et al. 2017; Model for Prediction Across Scales  
520 (MPAS), Skamarock et al. 2012; Ringler et al. 2013), will participate in aspects  
521 of CMIP6 (specifically OMIP and HighResMIP). CMIP6 will thus provide an  
522 excellent opportunity to assess and contrast such approaches within a large  
523 multi-model framework;

524

525 5. Improved physical parameterisations - particularly those that are designed to  
526 work at multiple scales (e.g. Arakawa et al. 2016; Fox-Kemper et al. 2013) - are  
527 being developed for all components of the climate system, but these efforts  
528 need resources and skilled people (Jakob 2014). Such schemes enable  
529 seamless modelling across space and timescale with less parameter tuning,  
530 albeit requiring the highest resolution global models for testing their efficacy.

531

532 *Observational requirements*

533 It is also important to exploit global observations that can both assess GCMs  
534 and explore independent ways to improve process representation, including  
535 their global teleconnections, in these models. An example is provided by the  
536 NASA Gravity Recovery And Climate Experiment (GRACE) satellite mission for  
537 the global water cycle (Böning et al. 2012), which is able to provide  
538 simultaneous assessment of water storage in different components of the  
539 climate system. The evolution of high-resolution GCMs represents an important  
540 and as yet unmet challenge to develop observational products at matching  
541 resolutions: no observational counterparts to the spatially complete and  
542 physically consistent GCMs exists, capable of supporting the study of multi-  
543 scale interactions. Instead, a wide range of instruments and methods, each with  
544 characteristic strengths and limitations, need to be employed. A combination of  
545 high resolution modeling and observational datasets are key to WCRP's Global  
546 Water and Energy Exchanges (GEWEX) project focus on improved  
547 understanding of the relevant geophysical processes of water and energy  
548 variability and change on regional to local scales.

549

550 At global resolutions affordable over the next decade, the representation of  
551 atmospheric convection remains a huge challenge. While it plays a fundamental  
552 role in the climate system, the poor quality of current simulations calls into  
553 question all processes dependent on it (including all Earth System complexity).  
554 This lack of simulation skill is also enveloped in many of the largest  
555 uncertainties in climate projections, such as climate sensitivity, in particular due  
556 to uncertainties in future cloud changes. However, even once model resolutions  
557 should become so refined that we may consider removing convective  
558 parameterisation, we would move into regimes in which poorly observed and  
559 understood interactions (multi-scale, aerosol-cloud-microphysics processes,  
560 air-sea and land-atmosphere interactions) will produce similar uncertainties.  
561 The number of ensemble simulations would also be severely limited, due to the  
562 huge computational expense. Hence there is no known threshold beyond which  
563 we would expect simulations to become independent of parameterisation  
564 choices, and therefore we need to continue to develop a manifold of global  
565 modelling practices, not limited to exploiting peak resolution.

566

567 [Summary](#)

568 Society requires robust information about climate risks over the next few  
569 decades in order to make good financial decisions about adaptation strategies,  
570 as well as mitigation decisions.

571

572 We have shown that enhanced resolution capabilities in global climate  
573 modelling have the potential to:

- 574 • provide improved, globally consistent information about climate hazards  
575 and impacts, as shown by examples pertinent to the global water cycle
- 576 • highlight future areas where more investment is required (High  
577 Performance Computing, better algorithms, suitable observations)
- 578 • use a common simulation protocol to enable deeper understanding

579

580 Tackling climate model uncertainty (measured by variability, or range of future  
581 projections) from different perspectives can potentially reveal limitations in any  
582 framework. We are moving forward with a suite of complementary efforts,  
583 spanning uniform grid refinement across the globe in CMIP-class models;  
584 improved dynamical mesh designs providing the foundations for cloud-system  
585 resolving simulations; unstructured mesh and stochastic approaches. We are  
586 implementing these changes at the present time, as part of CMIP6, and  
587 continued, albeit accelerated evolution should enable our future models to be  
588 significantly less dependent on still-unresolved processes, such as convection.

589

590 The computational and analysis cost of this new generation of simulations, in  
591 terms of HPC, storage, network speed and analysis platform, is clearly large.  
592 New collaborative paradigms will be needed to efficiently address some of  
593 these challenges, including use of central analysis platforms, incorporating both  
594 data storage and compute, so that algorithms can be moved to the data rather  
595 than vice versa. Better coordination of experimental design and collaboration  
596 can help to form multi-model datasets to ameliorate the cost of single model  
597 ensemble simulations, and greatly enhance the scientific understanding from  
598 community analyses of such datasets, using common tools. A current example  
599 of such good practice is CMIP6 HighResMIP.

600

## 601 APPENDIX A

## 602 Methodology to choose best model resolution

603 The methodology used to construct Figure 3 is based on the GA3 ensemble of  
604 global simulations (Mizielinski et al 2014), with five ensemble members at 25km  
605 and 130km resolution, and three members at 60km. Four observational  
606 datasets are used: Tropical Rainfall Measuring Mission 3B42 product, version  
607 7 (TRMM; Kummerow et al., 1998a; Huffman et al., 2007, 2010) and Climate  
608 Hazards Group InfraRed Precipitation with Station data (CHIRPS; Funk et al.  
609 2015) over 50°S-50°N, both at 25km grid resolution; Global Precipitation  
610 Climatology Centre (GPCC; Schneider et al. 2008) and the Global Precipitation  
611 Climatology Project (GPCP; Huffman et al. 2009), both globally at 110km. All  
612 data are initially regridded to a common 130km grid. For each region, a  
613 histogram of daily precipitation is constructed in two ways; a) using equally-  
614 spaced intensity bins, b) using a non-linear distribution of bins following Martin  
615 et al. (2017) to show the relative importance of precipitation events in a given  
616 intensity bin to the total precipitation. The root mean square difference (RMSD)  
617 between a reference histogram (TRMM in the tropics, GPCP in mid-high  
618 latitudes) and all other datasets is calculated across all bins using a logarithmic  
619 scale, and illustrated in Figure 5. Figure 3 is then determined by using the  
620 RMSD for each histogram type, to determine the coarsest best resolution model  
621 to fit the observations. When using different bins to calculate the RMSD  
622 produces contradictory results, or in regions where the observational datasets  
623 span a wider range than the model resolution differences, the “uncertain”  
624 category is used.

625

626 [Acknowledgments](#)

627 The authors would like to thank the reviewers and the editors for their efforts  
628 and constructive comments to improve the manuscript. We also thank many  
629 people for constructive comments, including Hiroyuki Murakami, Yohan  
630 Ruprich-Robert, Keith Williams and Dale Barker.

631 PRIMAVERA project members (MJR, PLV, HMC, SD, MED, RH, TJ, RS, CS,  
632 ES) acknowledge funding received from the European Commission under  
633 Grant Agreement 641727 of the Horizon 2020 research programme.

634 Met Office authors were supported by the Joint UK BEIS/Defra Met Office  
635 Hadley Centre Climate Programme (GA01101). RS acknowledges NERC-Met  
636 Office JWCRP HRCM funding. PLV, MED acknowledge NCAS Climate contract  
637 R8/H12/83/001 for the High Resolution Climate Modelling programme. MFW  
638 was supported by the Regional and Global Climate Modeling Program of the  
639 Office of Biological and Environmental Research in the Department of Energy  
640 Office of Science under contract DE-AC02-05CH11231. TJ has received  
641 funding from the European Union's Horizon 2020 Research & Innovation  
642 programme through grant agreement 727862 APPLICATE. HMC was  
643 supported by the European Research Council grant 291406. PC is supported  
644 by the US National Science Foundation grants AGS-146127 and AGS-  
645 1067937, and National Oceanic and Atmospheric Administration grant  
646 NA11OAR4310154, as well as by China's National Foundation of China  
647 (41490644 and U1406401). SMG acknowledges ongoing support from  
648 NOAA/GFDL. SM was supported by the Japan Society for the Promotion of  
649 Science (Grant-in-Aid for Scientific Research 22106008 and 22244057). MS  
650 was supported by the Strategic Programs for Innovative Research (SPIRE) and  
651 the FLAGSHIP2020 project of the Ministry of Education, Culture, Sports,  
652 Science and Technology, Japan. GS was supported by NASA Grants  
653 NNN13D984T and NNN12AA01C. TR was supported by the US Department of  
654 Energy Office of Science program for Scientific Discovery through Advanced  
655 Computing (SciDAC).

656

#### 657 [References:](#)

658

659 Ackerley, D., G. Berry, C. Jakob, M. J. Reeder, and J. Schwendike, 2015:  
660 Summertime precipitation over northern Australia in AMIP simulations from  
661 CMIP5. *Q. J. R. Meteorol. Soc.*, **141**, 1753–1768,  
662 <https://doi.org/10.1002/qj.2476>.

663

- 664 Adler, R.F., G. Gu, and G.J. Huffman, 2012: Estimating Climatological Bias  
665 Errors for the Global Precipitation Climatology Project (GPCP). *J. Appl. Meteor.*  
666 *Climatol.*, **51**, 84–99, <https://doi.org/10.1175/JAMC-D-11-052.1>.  
667
- 668 Arakawa, A., J.-H. Jung, and C.-M. Wu, 2016: Multiscale Modeling of the Moist-  
669 Convective Atmosphere. *Meteorol. Monogr.*, **56**, 16.1–16.17,  
670 <https://doi.org/10.1175/AMSMONOGRAPHS-D-15-0014.1>.  
671
- 672 Ban, N., J. Schmidli, and C. Schär, 2014: Evaluation of the convection-resolving  
673 regional climate modeling approach in decade-long simulations. *J. Geophys.*  
674 *Res. Atmos.* **119**, 7889–7907. <https://doi.org/10.1002/2014JD021478>.  
675
- 676 Banks, H. T., S. Stark, and A. B. Keen, 2007: The adjustment of the coupled  
677 climate model HadGEM1 towards equilibrium and the impact on global climate.  
678 *J. Clim.*, **20**, 5815–5826.  
679
- 680 Bauer, P., Thorpe, A., and Brunet, G., 2015: The quiet revolution of numerical  
681 weather prediction. *Nature*, **525**, 47–55. <https://doi.org/10.1038/nature14956>.  
682
- 683 Bechtold, P., N. Semane, Ph. Lopez, J.-P. Chaboureau, A. Beljaars, and N.  
684 Bormann, 2014: Representing Equilibrium and Nonequilibrium Convection in  
685 Large-Scale Models. *J. Atmos. Sci.*, **71**, 734–753.  
686
- 687 Bechtold, P., J.-P. Chaboureau, A. Beljaars, A. K. Betts, M. Köhler, M. Miller,,  
688 and J.-L. Redelsperger, 2004: The simulation of the diurnal cycle of convective  
689 precipitation over land in a global model. *Q.J.R. Meteorol. Soc.*, **130**, 3119–  
690 3137. <https://doi.org/10.1256/qj.03.103>.  
691
- 692 Bell, R., K. Hodges, P. L. Vidale, J. Strachan, and M. Roberts, 2014: Simulation  
693 of the global ENSO–Tropical cyclone teleconnection by a high-resolution  
694 coupled general circulation model. *J. Clim.*, **27**, 6404–6422, <https://doi.org/10.1175/JCLI-D-13-00559.1>.  
695  
696



697 Berckmans, J., T. Woollings, M.-E. Demory, P.-L. Vidale, and M. Roberts, 2013:  
698 Atmospheric blocking in a high resolution climate model: influences of mean  
699 state, orography and eddy forcing, *Atmos. Sci. Lett.*, **14**, 34–40,  
700 <https://doi.org/10.1002/asl2.412>.

701

702 Berner, J., and Coauthors, 2017: Stochastic Parameterization: Toward a New  
703 View of Weather and Climate Models. *Bull. Amer. Meteor. Soc.*, **98**, 565–  
704 588, <https://doi.org/10.1175/BAMS-D-15-00268.1>

705

706 Berner, J., K. R. Smith, S.-Y. Ha, J. Hacker, and C. Snyder, 2015: Increasing  
707 the skill of probabilistic forecasts: Understanding performance improvements  
708 from model-error representations, *Mon. Wea. Rev.*, **143**, 1295–1320.

709

710 Berner, J, T. Jung, and T. N. Palmer, 2012: Systematic model error: The impact  
711 of increased horizontal resolution versus improved stochastic and deterministic  
712 parameterizations. *J. Clim.*, **25**, 4946–4962.

713

714 Biastoch, A., C. W. Böning, and J. R. E. Lutjeharms, 2008: Agulhas leakage  
715 dynamics affects decadal variability in Atlantic overturning circulation. *Nature*,  
716 **456**, 489-492, <https://doi.org/10.1038/nature07426>.

717

718 Birch, C. E., M. Roberts, L. Garcia-Carreras, D. Ackerley, M. Reeder, and A.  
719 Lock, 2015: Sea breeze dynamics and convection initiation: the influence of  
720 convective parameterisation on model biases, *J. Clim.*, **28**, 8093–8108,  
721 <https://doi.org/10.1175/JCLI-D-14-00850.1>.

722

723 Böning, C., J. K. Willis, F. W. Landerer, R. S. Nerem, and J. Fasullo, 2012: The  
724 2011 La Niña: So strong, the oceans fell. *Geophys. Res. Lett.*, **39**, L19602,  
725 <https://doi.org/10.1029/2012gl053055>.

726

727 Böning, C. W., E. Behrens, A. Biastoch, K. Getzlaff, and J. L. Bamber, 2016.  
728 Emerging impact of Greenland meltwater on deepwater formation in the North  
729 Atlantic Ocean. *Nat. Geosci.*, **9**, 523–527, <https://doi.org/10.1038/ngeo2740>.

730

- 731 Brown, A., Milton, S., Cullen, M., Golding, B., Mitchell, J., Shelly, A., 2012.  
732 Unified modeling and prediction of weather and climate: A 25-year journey. *Bull.*  
733 *Amer. Meteor. Soc.*, **93**, 1865–1877. doi:10.1175/BAMS-D-12-00018.1.  
734
- 735 Bryan, F. O., R. Tomas, J. M. Dennis, D. B. Chelton, N. G. Loeb, and J. L.  
736 McClean, 2010: Frontal scale air–sea interaction in high-resolution coupled  
737 climate models. *J. Clim.*, **23**, 6277–6291.  
738
- 739 Camp, J., M. Roberts, C. MacLachlan, E. Wallace, L. Hermanson, A.  
740 Brookshaw, A. Arribas, and A. Scaife, 2015: Seasonal forecasting of tropical  
741 storms using the Met Office high resolution seasonal forecast system. *Q. J. R.*  
742 *Meteor. Soc.*, **141**, 2206–2219. <https://doi.org/ht10.1002/qj.2516>.  
743
- 744 Caron, L.-P., C. G. Jones, and K. Winger, 2011: Impact of resolution and  
745 downscaling technique in simulating recent Atlantic tropical cyclone activity.  
746 *Clim. Dyn.*, **37**, 869–892, <https://doi.org/10.1007/s00382-010-0846-7>.  
747
- 748 Catto, J, L. C. Shaffrey, and K. I. Hodges, 2010: Can climate models capture  
749 the structure of extratropical cyclones? *J. Clim.*, **23**, 1621-1635,  
750 <https://doi.org/10.1175/2009JCLI3318.1>.  
751
- 752 Chelton D. B. and S.-P. Xie, 2010: Coupled ocean–atmosphere interaction at  
753 oceanic mesoscales. *Oceanography*, **23**, 52–69.  
754
- 755 Chelton, D. B., M. G. Schlax, M. H. Freilich, and R. F. Milliff, 2004: Satellite  
756 measurements reveal persistent small-scale features in ocean winds. *Science*,  
757 **303**, 978–983.  
758
- 759 Chelton, D. B., and Coauthors, 2001: Observations of coupling between surface  
760 wind stress and sea surface temperature in the eastern tropical Pacific. *J. Clim.*,  
761 **14**, 17,877–17,904.  
762

763 Christensen, H. M., J. Berner, D. R. Coleman, and T. N.  
764 Palmer, 2017: Stochastic Parameterization and El Niño–Southern  
765 Oscillation. *J. Clim.*, **30**, 17–38, <https://doi.org/10.1175/JCLI-D-16-0122.1>.

766

767 Christensen, H. M., I. M. Moroz, and T. N. Palmer, 2015. Simulating Weather  
768 Regimes: impact of stochastic and perturbed parameter schemes in a simple  
769 atmospheric model. *Clim. Dyn.* **44**, 2195-2214.

770

771 Clark, A. J., W. A. Gallus Jr., and T.-C. Chen, 2007: Comparison of the diurnal  
772 precipitation cycle in convection-resolving and non-convection-resolving  
773 mesoscale models. *Mon. Wea. Rev.*, **135**, 3456–3473,  
774 <https://doi.org/10.1175/MWR3467.1>.

775

776 Collins, M., Minobe, S., Barreiro, M., Bordoni, S., Kaspi, Y., Kuwano-Yoshida,  
777 A., Keenlyside, N., Manzini, E., O'Reilly, C.H., Sutton, R., Xie, S.P., Zolina, O.,  
778 2018: Challenges and opportunities for improved understanding of regional  
779 climate dynamics. *Nature Clim. Cha.* **8**, 101–108.  
780 <https://doi.org/10.1038/s41558-017-0059-8>.

781

782 Danilov, S., 2013: Ocean modelling on unstructured meshes. *Ocean Modelling*,  
783 **69**, 195-210.

784

785 Danilov, S., D. Sidorenko, Q. Wang, and T. Jung, 2017: The Finite-volume Sea  
786 ice–Ocean Model (FESOM2). *Geosci. Model Dev.*, **10**, 765–789,  
787 <https://doi.org/10.5194/gmd-10-765-2017>.

788

789 Dawson, A. and T. N. Palmer, 2015: Simulating weather regimes: impact of  
790 model resolution and stochastic parameterization. *Clim. Dyn.*, **44**, 2177.  
791 <https://doi.org/10.1007/s00382-014-2238-x>.

792

793 Dawson, A., T. N. Palmer, and S. Corti, 2012: Simulating regime structures in  
794 weather and climate prediction models. *Geophys. Res. Lett.*, **39**, L21805,  
795 <https://doi.org/10.1029/2012GL053284>.

796

- 797 Delworth, T.L., and Coauthors, 2012: Simulated climate and climate change in  
798 the GFDL CM2.5 high-resolution coupled climate model, *J. Clim.*, **25**, 2755–  
799 2781, <https://doi.org/10.1175/JCLI-D-11-00316.1>.  
800
- 801 Demory, M.-E., P. L. Vidale, M. J. Roberts, P. Berrisford, J. Strachan, R.  
802 Schiemann, and M. S. Mizieliński, 2014: The role of horizontal resolution in  
803 simulating drivers of the global hydrological cycle. *Clim. Dyn.*, **42**, 2201–2225.  
804
- 805 Dorrestijn, J., D.T. Crommelin, A.P. Siebesma, and H. J. J. Jonker, 2013: *Theor.*  
806 *Comput. Fluid Dyn.*, **27**, 133. <https://doi.org/10.1007/s00162-012-0281-y>.  
807
- 808 Eyring, V., S. Bony, G. A. Meehl, C. A. Senior, B. Stevens, R. J. Stouffer, and  
809 K. E. Taylor, 2016: Overview of the Coupled Model Intercomparison Project  
810 Phase 6 (CMIP6) experimental design and organization. *Geosci. Model Dev.*,  
811 **9**, 1937–1958, <https://doi.org/10.5194/gmd-9-1937-2016>.  
812
- 813 Flato, G., and Coauthors, 2013: Evaluation of climate models. *Climate Change*  
814 *2013: The Physical Science Basis*, T. F. Stocker et al., Eds., Cambridge  
815 University Press, 741–866.  
816
- 817 Fox-Kemper, B., S. Bachman, B. Pearson, and S. Reckinger, 2014: Principles  
818 and advances in subgrid modeling for eddy-rich simulations. *CLIVAR*  
819 *Exchanges*. **65**, 2.  
820
- 821 Frankignoul, C., N. Sennéchal, Y.-O. Kwon, and M. A. Alexander, 2011:  
822 Influence of the Meridional Shifts of the Kuroshio and the Oyashio Extensions  
823 on the Atmospheric Circulation. *J. Clim.*, **24**, 762–777.  
824
- 825 Frenger, I., N. Gruber, R. Knutti, and M. Munnich, 2013: Imprint of Southern  
826 Ocean eddies on winds, clouds and rainfall. *Nat. Geosci.*, **6**, 608–612.  
827
- 828 Funk, C., and Coauthors, 2015: The climate hazards infrared precipitation with  
829 stations—a new environmental record for monitoring extremes. *Sci. Data* **2**,  
830 150066, <https://doi.org/10.1038/sdata.2015.66>.

831

832 Gao, Y., L. R. Leung, E. P. S. Jr., F. Dominguez, B. Nijssen, and D. P.  
833 Lettenmaier, 2012: Moisture flux convergence in regional and global climate  
834 models: Implications for droughts in the southwestern United States under  
835 climate change. *Geophys. Res. Lett.*, **39**, L09711.

836

837 Griffies, S. M., and Coauthors, 2015: Impacts on ocean heat from transient  
838 mesoscale eddies in a hierarchy of climate models, *J. Clim.*, **28**, 952-977,  
839 <https://doi.org/10.1175/JCLI-D-14-00353.1>.

840

841 Guo, L., N. P. Klingaman, P. L. Vidale, A. G. Turner, M.-E. Demory, and  
842 A. Cobb, 2017: Contribution of Tropical Cyclones to Atmospheric Moisture  
843 Transport and Rainfall over East Asia. *J. Clim.*, **30**, 3853-3865,  
844 <https://doi.org/10.1175/JCLI-D-16-0308.1>.

845

846 Haarsma, R. J., and Coauthors, 2016: High Resolution Model Intercomparison  
847 Project (HighResMIP), *Geosci. Model Dev.*, **9**, 4185-4208,  
848 <https://doi.org/10.5194/gmd-2016-66>.

849

850 Haarsma, R. J., W. Hazeleger, C. Severijns, H. de Vries, A. Sterl, R. Bintanja,  
851 G. J. van Oldenborgh, and H. W. van den Brink, 2013: More hurricanes to hit  
852 western Europe due to global warming, *Geophys. Res. Lett.*, **40**, 1783–1788,  
853 <https://doi.org/10.1002/grl.50360>.

854

855 Hack, J. J., J. M. Caron, G. Danabasoglu, and K. W. Oleson, 2006: CCSM-  
856 CAM3 Climate Simulation Sensitivity to Changes in Horizontal Resolution. *J.*  
857 *Clim.*, **19**, 2267–2289.

858

859 Hagemann, S., K. Arpe, and E. Roeckner, 2006: Evaluation of the hydrological  
860 cycle in the ECHAM5 model. *J. Clim.*, **19**, 3810–3827.

861

862 Hallberg, R.W., 2013: Using a resolution function to regulate parameterizations  
863 of oceanic mesoscale eddy effects. *Ocean Modelling*, **72**, 92-103,

864 <https://doi.org/10.1016/j.ocemod.2013.08.007>.

865

866 Hashino, T., M. Satoh, Y. Hagihara, T. Kubota, T. Matsui, T. Nasuno, and H.  
867 Okamoto, 2013: Evaluating Global Cloud Distribution and Microphysics from  
868 the NICAM against CloudSat and CALIPSO. *J. Geophys. Res.*, **118**, 7273-  
869 7292, <https://doi.org/10.1002/jgrd.50564>.

870

871 Hawcroft, M., L. Shaffrey, K. Hodges, and H. Dacre, 2016: Can climate models  
872 represent the precipitation associated with extratropical cyclones? *Clim. Dyn.*,  
873 **47**, 679-695, <https://doi.org/10.1007/s00382-015-2863-z>.

874

875 Hawcroft, M., H. Dacre, R. K. Forbes, Hodges, L. Shaffrey, and T. Stein, 2017:  
876 Using satellite and reanalysis data to evaluate the representation of latent  
877 heating in extratropical cyclones in a climate model. *Clim. Dyn.*, **48**, 2255-2278,  
878 <https://doi.org/10.1007/s00382-016-3204-6>.

879

880 Hewitt, H. T., and Coauthors, 2016: The impact of resolving the Rossby radius  
881 at mid-latitudes in the ocean: results from a high-resolution version of the Met  
882 Office GC2 coupled model. *Geosci. Model Dev.*, **9**, 3655-3670,  
883 <https://doi.org/10.5194/gmd-2016-87>.

884 Hewitt, H. T., and Coauthors, 2017: Will high-resolution global ocean models  
885 benefit coupled predictions on short-range to climate timescales? *Ocean*  
886 *Modelling*, accepted.

887 Huffman, G.J, R.F. Adler, D.T. Bolvin, and G. Gu, 2009: Improving the Global  
888 Precipitation Record: GPCP Version 2.1. *Geophys. Res. Lett.*, **36**, L17808,  
889 <https://doi.org/10.1029/2009GL040000>.

890

891 Huffman, G. J., R. F. Adler, D. T. Bolvin, G. Gu, E. J. Nelkin, K. P. Bowman, Y.  
892 Hong, E. F. Stocker, and D. B. Wolff, 2007: The TRMM multi-satellite  
893 precipitation analysis: quasi-global, multiyear, combined-sensor precipitation  
894 estimates at fine scale, *J. Hydrometeorol.*, **8**, 38–55.

895

- 896 Huffman, G. J., R. F. Adler, D. T. Bolvin, and E. J. Nelkin, 2010: The TRMM  
897 multi-satellite precipitation analysis (TMPA). *Satellite rainfall applications for*  
898 *surface hydrology*, F. Hossain, and M. Gebremichael, Ed., 3–22, Springer  
899 Verlag.
- 900
- 901 Jakob, C., 2014: Going back to basics. *Nat. Clim. Change*, **4**, 1042-1045,  
902 <https://doi.org/10.1038/nclimate2445>.
- 903
- 904 Johnson, S. J., and Coauthors, 2016: The resolution sensitivity of the South  
905 Asian monsoon and Indo-Pacific in a global 0.35° AGCM. *Clim. Dyn.*, **46**(3–4),  
906 807–831, <https://doi.org/10.1007/s00382-015-2614-1>.
- 907
- 908 Jung, T., T. N. Palmer, and G. J. Shutts, 2005: Influence of a stochastic  
909 parameterization on the frequency of occurrence of North Pacific weather  
910 regimes in the ECMWF model. *Geophys. Res. Lett.*, **32**, L23811,  
911 <https://doi.org/10.1029/2005GL024248>.
- 912
- 913 Jung, T., and Coauthors, 2012: High-Resolution Global Climate Simulations  
914 with the ECMWF Model in Project Athena: Experimental Design, Model Climate,  
915 and Seasonal Forecast Skill. *J. Clim.*, **25**, 3155–3172,  
916 <https://doi.org/10.1175/JCLI-D-11-00265.1>.
- 917
- 918 Kendon E.J., N. Ban, N.M. Roberts, H.J. Fowler, M.J. Roberts, S.C. Chan, J.P.  
919 Evans, G. Fosser and J. M. Wilkinson, 2017: Do convection-permitting regional  
920 climate models improve projections of future precipitation change? *Bull. Amer.*  
921 *Meteor. Soc.*, **98**, 79-93, <https://doi.org/10.1175/BAMS-D-15-0004.1>.
- 922
- 923 Kirtman, B. P., and Coauthors, 2012: Impact of ocean model resolution on  
924 CCSM climate simulations, *Clim. Dyn.*, **39**, 1303–1328,  
925 <https://doi.org/10.1007/s00382-012-1500-3>.
- 926
- 927 Kodama, C., and Coauthors, 2015: A 20-year climatology of a NICAM AMIP-  
928 type simulation. *J. Meteor. Soc. Japan*, **93**, 393-424,  
929 <https://doi.org/10.2151/jmsj.2015-024>.

930

931 Kuhlbrodt, T, J. M. Gregory and L. C. Shaffrey, 2015: A process-based analysis  
932 of ocean heat uptake in an AOGCM with an eddy-permitting ocean component.  
933 *Clim. Dyn.*, **45**, 3205-3226, <https://doi.org/10.1007/s00382-015-2534-0>

934

935 Kummerow, C., W. Barnes, T. Kozu, J. Shiue, and J. Simpson, 1998: The  
936 Tropical Rainfall Measuring Mission (TRMM) sensor package, *J. Atmos.*  
937 *Ocean. Tech.*, **15**, 809–817.

938

939 Kuwano-Yoshida, A., S. Minobe, and S.-P. Xie, 2010: Precipitation response to  
940 the Gulf Stream in an atmospheric GCM. *J. Clim.*, **23**, 3676-3698.

941

942 Kuwano-Yoshida A., and S. Minobe, 2017: Storm track response to SST front  
943 in the northwestern Pacific region in an AGCM. *J. Clim.*, **30**, 1081-1102.

944

945 Kwon, Y.-O., M. A. Alexander, N. A. Bond, C. Frankignoul, H. Nakamura, B.  
946 Qiu, and L. A. Thompson, 2010: Role of the Gulf Stream and Kuroshio–Oyashio  
947 Systems in Large-Scale Atmosphere–Ocean Interaction: A Review. *J. Clim.*,  
948 **23**, 3249-3281.

949

950 Lau, W. K. and K.-M. Kim, 2012: The 2010 Pakistan Flood and Russian Heat  
951 Wave: Teleconnections of Hydrometeorological Extremes. *J. Hydrometeorol.*,  
952 **13**, 392-403, <https://doi.org/10.1175/JHM-D-11-016.1>.

953

954 Levine, R.C. and G. M. Martin, 2017: On the climate model simulation of Indian  
955 monsoon low pressure systems and the effect of remote disturbances and  
956 systematic biases. *Clim. Dyn.*, <https://doi.org/10.1007/s00382-017-3900-x>.

957

958 Lin, J. W.-B., and J. D. Neelin, 2003: Toward stochastic deep convective  
959 parameterization in general circulation models, *Geophys. Res. Lett.*, **30**, 1162,  
960 <https://doi.org/10.1029/2002GL016203>.

961



- 962 Lin, J. W.-B., and J. D. Neelin, 2000: Influence of a stochastic moist convective  
963 parameterization on tropical climate variability, *Geophys. Res. Lett.*, **27**, 3691–  
964 3694.
- 965
- 966 Ma, J., H. Xu, C. Dong, P. Lin, and Y. Liu, 2015: Atmospheric responses to  
967 oceanic eddies in the Kuroshio Extension region, *J. Geophys. Res.*, **120**, 6313-  
968 6330, [https://doi.org/ 10.1002/2014JD022930](https://doi.org/10.1002/2014JD022930).
- 969
- 970 Ma, X., and Coauthors, 2015: Distant Influence of Kuroshio Eddies on North  
971 Pacific Weather Patterns? *Sci. Rep.*, **5**. 17785.
- 972
- 973 Ma, X., and Coauthors, 2016: Importance of Resolving Kuroshio Front and  
974 Eddy Influence in Simulating North Pacific Storm Track, *J. Clim.*, **30**, 1861-1880,  
975 <https://doi.org/10.1175/JCLI-D-16-0154.1>.
- 976
- 977 Magnusson, L., and Källén, E., 2013: Factors Influencing Skill Improvements in  
978 the ECMWF Forecasting System. *Mon. Wea. Rev.*, **141**, 3142–3153.  
979 <https://doi.org/10.1175/MWR-D-12-00318.1>.
- 980
- 981 Maloney E. D. and D. B. Chelton, 2006: An assessment of the sea surface  
982 temperature influence on surface wind stress in numerical weather prediction  
983 and climate models. *J. Clim.*, **19**, 2743-2762.
- 984
- 985 Manganello, J. V., and Coauthors, 2012: Tropical cyclone climatology in a 10-  
986 km global atmospheric GCM: Toward weather resolving climate modeling. *J.*  
987 *Clim.*, **25**, 3867–3893, <https://doi.org/10.1175/JCLI-D-11-00346.1>.
- 988
- 989 Martin, E. R., and C. Thorncroft, 2015: Representation of African Easterly  
990 waves in CMIP5 models. *J. Clim.*, **28**, <https://doi.org/10.1175/JCLI-D-15-0145.1>.
- 991
- 992 Martin, G. M., S. F. Milton, C. A. Senior, M. E. Brooks, S. Ineson, T. Reichler  
993 and J. Kim, 2010: Analysis and Reduction of Systematic Errors through a  
994 Seamless Approach to Modelling Weather and Climate. *J. Clim.*, **23**, 5933-5957,  
995 <https://doi.org/10.1175/2010JCLI3541.1>.

996  
997 Martin, G. M., N. P. Klingaman and A. F. Moise, 2017: Connecting spatial and  
998 temporal scales of tropical precipitation in observations and the MetUM-GA6.  
999 *Geosci. Model Dev.*, **10**, 105-126, <https://doi.org/10.5194/gmd-10-105-2017>.  
1000  
1001 Masunaga, R., H. Nakamura, T. Miyasaka, K. Nishii, and Y. Tanimoto, 2015:  
1002 Separation of climatological imprints of the Kuroshio Extension and Oyashio  
1003 fronts on the wintertime atmospheric boundary layer: Their sensitivity to SST  
1004 resolution prescribed for atmospheric reanalysis. *J. Clim.*, **28**, 1764–1787.  
1005  
1006 Matsueda, M., and T. N. Palmer, 2011. Accuracy of climate change predictions  
1007 using high resolution simulations as surrogates of truth. *Geophys. Res. Lett.*,  
1008 **38**, L05803.  
1009  
1010 McClean, J. L., and Coauthors, 2011: A prototype two-decade fully-coupled  
1011 fine-resolution CCSM simulation. *Ocean Modell.*, **39**, 10–30.  
1012  
1013 McKiver, W. J., M. Vichi, T. Lovato, A. Storto, S. Masina, 2015: Impact of  
1014 increased grid resolution on global marine biogeochemistry. *J. Mar. Sys.*, **147**,  
1015 153-168, <https://doi.org/10.1016/j.jmarsys.2014.10.003>.  
1016  
1017 Meehl, G.A., C. Covey, T. L. Delworth, M. Latif, B. McAveney, J. F. B. Mitchell,  
1018 R. J. Stouffer, and K. E. Taylor, 2007: The WCRP CMIP3 multimodel dataset:  
1019 A new era in climate change research. *Bull. Amer. Meteor. Soc.*, **88**, 1383–  
1020 1394, <https://doi.org/10.1175/BAMS-88-9-1383>.  
1021  
1022 Meehl, G. A., G. J. Boer, C. Covey, M. Latif, and R. J. Stouffer, 2000: The  
1023 Coupled Model Intercomparison Project (CMIP). *Bull. Amer. Meteor. Soc.*, **81**,  
1024 313-318.  
1025  
1026 Minobe. S., A. Kuwano-Yoshida, N. Komori, S.-P. Xie, and R. J. Small, 2008:  
1027 Influence of the Gulf Stream on the troposphere. *Nature*, **452**, 206-209.  
1028

- 1029 Minobe, S., M. Miyashita, A. Kuwano-Yoshida, H. Tokinaga, and S.-P. Xie,  
1030 2010: Atmospheric response to the Gulf Stream: Seasonal variations. *J. Clim.*,  
1031 **23**, 3699–3719.
- 1032
- 1033 Mittermaier, M., North, R., Semple, A., & Bullock, R., 2016: Feature-Based  
1034 Diagnostic Evaluation of Global NWP Forecasts. *Mon. Wea. Rev.*, **144**, 3871–  
1035 3893. <https://doi.org/10.1175/MWR-D-15-0167.1>.
- 1036
- 1037 Miura, H., Satoh, M., Nasuno, T., Noda, A.T., and Oouchi, K., 2007: A Madden-  
1038 Julian Oscillation event simulated using a global cloud-resolving model.  
1039 *Science*, **318**, 1763-1765.
- 1040
- 1041 Miyakawa, T., Y. N. Takayabu, T. Nasuno, H. Miura, M. Satoh, M. W. Moncrieff,  
1042 2012: Convective momentum transport by rainbands within a Madden-Julian  
1043 oscillation in a global nonhydrostatic model with explicit deep convective  
1044 processes. Part I: Methodology and general results. *J. Atmos. Sci.*, **69**, 1317-  
1045 1338.
- 1046
- 1047 Miyamoto, Y., Y. Kajikawa, R. Yoshida, T. Yamaura, H. Yashiro, and H. Tomita,  
1048 2013: Deep moist atmospheric convection in a subkilometer global simulation.  
1049 *Geophys. Res. Lett.*, **40**, 4922-4926, <https://doi.org/10.1002/grl.50944>.
- 1050
- 1051 Mizielinski, M. S., and Coauthors, 2014: High resolution global climate  
1052 modelling; the UPSCALE project, a large simulation campaign. *Geosci. Model*  
1053 *Dev.*, **7**, 563–591, <https://doi.org/10.5194/gmdd-7-563-2014>.
- 1054
- 1055 Murakami, H., G. Villarini, G. A. Vecchi, W. Zhang, and R. G. Gudgel, 2016:  
1056 Statistical–Dynamical Seasonal Forecast of North Atlantic and U.S. Landfalling  
1057 Tropical Cyclones Using the High-Resolution GFDL FLOR Coupled Model.  
1058 *Mon. Weather Rev.*, **144**, 2101-2123, [https://doi.org/10.1175/MWR-D-15-](https://doi.org/10.1175/MWR-D-15-0308.1)  
1059 0308.1.
- 1060
- 1061 Murakami H., and Coauthors, 2015: Simulation and Prediction of Category 4  
1062 and 5 Hurricanes in the High-Resolution GFDL HiFLOR Coupled Climate

1063 Model: *J. Clim.* **28**, 9058-9079.  
1064  
1065 Nakano, M., and Coauthors, 2017: Global 7-km mesh nonhydrostatic Model  
1066 Intercomparison Project for improving TYphoon forecast (TYMIP-G7):  
1067 Experimental design and preliminary results. *Geosci. Model Dev.*, **10**, 1363-  
1068 1381, <https://doi.org/10.5194/gmd-2016-184>.  
1069  
1070 Nakano, M., M. Sawada, T. Nasuno, M. Satoh, 2015: Intraseasonal variability  
1071 and tropical cyclogenesis in the western North Pacific simulated by a global  
1072 nonhydrostatic atmospheric model. *Geophys. Res. Lett.*, **42**, 565-571,  
1073 <https://doi.org/10.1002/2014GL062479>.  
1074  
1075 Ogata, T., S. J. Johnson, R. Schiemann, M.-E. Demory, R. Mizuta, K.  
1076 Yoshida, O. Arakawa, 2017: The resolution sensitivity of the Asian summer  
1077 monsoon and its inter-model comparison between MRI-AGCM and MetUM.  
1078 *Clim. Dyn.*, <https://doi.org/10.1007/s00382-016-3517-5>.  
1079  
1080 O'Reilly, C. H., and A. Czaja, 2015: The response of the Pacific storm track  
1081 and atmospheric circulation to Kuroshio Extension variability. *Q. J. R.*  
1082 *Meteorol. Soc.*, **141**, 52-66.  
1083  
1084 O'Reilly, C. H., S. Minobe, A. Kuwano-Yoshida, 2016: The influence of the  
1085 Gulf Stream on wintertime European blocking. *Clim. Dyn.*, **47**, 1545-1567,  
1086 <https://doi.org/10.1007/s00382-015-2919-0>  
1087  
1088 O'Reilly, C. H. S. Minobe, A. Kuwano-Yoshida, and T. Woollings, 2017: The  
1089 Gulf Stream influence on wintertime North Atlantic jet variability. *Q. J. R.*  
1090 *Meteorol. Soc.*, **143**, 173-183.  
1091  
1092 Palmer, T., R. Buizza, F. Doblas-Reyes, T. Jung, M. Leutbecher, G. Shutts, M.  
1093 Steinheimer, and A. Weisheimer, 2009: Stochastic parametrization and model  
1094 uncertainty. Tech. Rep. ECMWF RD Tech. Memo. 598, 42 pp,  
1095 <http://www.ecmwf.int/publications/>.  
1096

- 1097 Pantillon, F., J.-P. Chaboureau, and E. Richard, 2015: Remote impact of North  
1098 Atlantic hurricanes on the Mediterranean during episodes of intense rainfall in  
1099 autumn 2012. *Q. J. R. Meteorol. Soc.*, **141**, 967–978,  
1100 <https://doi.org/10.1002/qj.2419>.  
1101
- 1102 Parfitt, R., A. Czaja, S. Minobe, and A. Kuwano-Yoshida, 2016: The  
1103 atmospheric frontal response to SST perturbations in the Gulf Stream region,  
1104 *Geophys. Res. Lett.*, **43**, 2299–2306, <https://doi.org/10.1002/2016GL067723>.  
1105
- 1106 Piazza M., L. Terray, J. Boé, E. Maisonnave, E. Sanchez-Gomez, 2015:  
1107 Influence of small-scale North Atlantic sea surface temperature patterns on the  
1108 marine boundary layer and free troposphere: a study using the atmospheric  
1109 ARPEGE model. *Clim. Dyn.*, **46**, 1699-1717.  
1110
- 1111 Pope, V. D. and R. A. Stratton, 2002. The processes governing horizontal  
1112 resolution sensitivity in a climate model. *Clim. Dyn.*, **19**, 211–236.  
1113
- 1114 Puy M., and Coauthors, 2017: Influence of Westerly Wind Events stochasticity  
1115 on El Niño amplitude: the case of 2014 vs. 2015. *Clim. Dyn.*, in press.  
1116
- 1117 Ringler, T., M. Petersen, R. L. Higdon, D. Jacobsen, P. W. Jones, and M.  
1118 Maltrud, 2013: A Multi-Resolution Approach to Global Ocean Modeling. *Ocean*  
1119 *Modell.* **69**(C), 211–232. <https://doi.org/10.1016/j.ocemod.2013.04.010>.  
1120
- 1121 Roberts, M. J., H. T. Hewitt, P. Hyder, D. Ferreira, S. A. Josey, M. Mizielinski,  
1122 and A. Shelly, 2016: Impact of ocean resolution on coupled air-sea fluxes and  
1123 large-scale climate. *Geophys. Res. Lett.*, **43**,  
1124 <https://doi.org/10.1002/2016GL070559>.  
1125
- 1126 Roberts, M. J., and Coauthors, 2015: Tropical cyclones in the UPSCALE  
1127 ensemble of high-resolution global climate models. *J. Clim.*, **28**, 574–596,  
1128 <https://doi.org/10.1175/JCLI-D-14-00131.1>.  
1129

- 1130 Rodwell, M. J., Richardson, D. S., Hewson, T. D., and Haiden, T., 2010: A new  
1131 equitable score suitable for verifying precipitation in numerical weather  
1132 prediction. *Q. J. R. Meteorol. Soc.*, **136**, 1344-1363.  
1133 <https://doi.org/10.1002/qj.656>.  
1134
- 1135 Saba, V. S., and Coauthors, 2016: Enhanced warming of the Northwest Atlantic  
1136 Ocean under climate change, *J. Geophys. Res. Oceans*, **121**, 118–132,  
1137 <https://doi.org/10.1002/2015JC011346>.  
1138
- 1139 Satoh, M., T. Matsuno, H. Tomita, H. Miura, T. Nasuno, S. Iga, 2008:  
1140 Nonhydrostatic Icosahedral Atmospheric Model (NICAM) for global cloud  
1141 resolving simulations. *J. Comp. Phys.*, **227**, 3486-3514,  
1142 <https://doi.org/10.1016/j.jcp.2007.02.006>.  
1143
- 1144 Satoh, M., and Coauthors, 2014: The Non-hydrostatic Icosahedral Atmospheric  
1145 Model: Description and development. *Prog. Earth Planet. Sci.*, **1**, 18,  
1146 <https://doi.org/10.1186/s40645-014-0018-1>.  
1147
- 1148 Scaife, A. A., D. Copsey, C. Gordon, C. Harris, T. Hinton, S. Keeley, A. O'Neill,  
1149 M. Roberts, and K. Williams, 2011: Improved Atlantic winter blocking in a  
1150 climate model, *Geophys. Res. Lett.*, **38**, L23703,  
1151 <https://doi.org/10.1029/2011GL049573>.  
1152
- 1153 Scher, S., R. J. Haarsma, H. de Vries, S. S. Drijfhout, and A. J. van Delden,  
1154 2017: Resolution dependence of extreme precipitation and deep convection  
1155 over the Gulf Stream, *J. Adv. Model. Earth Syst.*, **9**, 1186–1194,  
1156 <https://doi.org/10.1002/2016MS000903>.  
1157
- 1158 Schiemann, R., and Coauthors, 2016: The resolution sensitivity of Northern  
1159 Hemisphere blocking in four 25-km atmospheric global circulation models. *J.*  
1160 *Clim.*, **30**, 337-358, <https://doi.org/10.1175/JCLI-D-16-0100.1>.  
1161
- 1162 Schneider, T., J. Teixeira, C. S. Bretherton, F. Brient, K. G. Pressel, C. Schär,  
1163 A. P. Siebesma, 2017: Climate goals and computing the future of clouds. *Nat.*

- 1164 *Clim. Change*, **7**, 3–5, <https://doi.org/10.1038/nclimate3190>.
- 1165
- 1166 Schneider, U., T. Fuchs, A. Meyer-Christoffer and B. Rudolf, 2008: Global  
1167 Precipitation Analysis Products of the GPCC. *Global Precipitation Climatology*  
1168 *Centre (GPCC)*, DWD, Internet Publikation, 1-12.
- 1169
- 1170 Scoccimarro, E., S. Gualdi, and A. Navarra, 2012: Tropical cyclone effects on  
1171 Arctic Sea ice variability, *Geophys. Res. Lett.*, **39**, L17704,  
1172 <https://doi.org/10.1029/2012GL052987>.
- 1173
- 1174 Scoccimarro E., S. Gualdi, G. Villarini, G. Vecchi, M. Zhao, K. Walsh, A.  
1175 Navarra, 2014: Intense precipitation events associated with landfalling tropical  
1176 cyclones in response to a warmer climate and increased CO<sub>2</sub>. *J. Clim.*, **27**,  
1177 4642-4654, <https://doi.org/10.1175/JCLI-D-14-00065.1>.
- 1178
- 1179 Scoccimarro E., 2016: Modelling Tropical Cyclones in a changing climate.  
1180 Oxford Research Encyclopedia of Natural Hazard Science. [https://doi.org/](https://doi.org/10.1093/acrefore/9780199389407.013.22)  
1181 [10.1093/acrefore/9780199389407.013.22](https://doi.org/10.1093/acrefore/9780199389407.013.22). Oxford University Press.
- 1182
- 1183 Scoccimarro E., P.G. Fogli, K. Reed, S. Gualdi, S. Masina, and A. Navarra,  
1184 2017: Tropical cyclone interaction with the ocean: the role of high frequency  
1185 (sub-daily) coupled processes. *J. Clim.*, **30**, 145–162,  
1186 <https://doi.org/10.1175/JCLI-D-16-0292.1>
- 1187
- 1188 Sein, D. V., S. Danilov, A. Biastoch, J. V. Durgadoo, D. Sidorenko, S. Harig,  
1189 and Q. Wang, 2016: Designing variable ocean model resolution based on the  
1190 observed ocean variability, *J. Adv. Model. Earth Syst.*, **8**,  
1191 <https://doi.org/10.1002/2016MS000650>.
- 1192
- 1193 Senior, C.A., A. Arribas, A.R. Brown, M.J.P. Cullen, T.C. Johns, G.M. Martin,  
1194 S.F. Milton, D.M. Smith, S. Webster and K.D. Williams, 2009: Synergies  
1195 between Numerical Weather Prediction and General Circulation Climate  
1196 Models. Chapter for "The Development of Atmospheric General Circulation  
1197 Models". Donner, L., Schubert, W. and Somerville, R. Eds. ISBN 978-0-521-

1198 19006-0  
1199  
1200 Skamarock, W. C., J. B. Klemp, M. G. Duda, L. Fowler, S.-H. Park, and T. D.  
1201 Ringler, 2012: A Multi-scale Nonhydrostatic Atmospheric Model Using  
1202 Centroidal Voronoi Tessellations and C-Grid Staggering. *Mon. Weath. Rev.*,  
1203 **240**, 3090-3105, <https://doi.org/10.1175/MWR-D-11-00215.1>  
1204  
1205 Slingo, J. M., K. R. Sperber, J.-J. Morcrette, and G. L. Potter, 1992: Analysis of  
1206 the temporal behavior of convection in the tropics of the European Centre for  
1207 Medium-Range Weather Forecasts model, *J. Geophys. Res.*, **97**(D16), 18119–  
1208 18135, <https://doi.org/10.1029/92JD01408>.  
1209  
1210 Small, R.J., and Coauthors, 2014a: A new synoptic-scale resolving global  
1211 climate simulation using the Community Earth System Model. *J. Adv. Mod.*  
1212 *Earth Sys*, **6**, 1065-1094, <https://doi.org/10.1002/2014MS000363>.  
1213  
1214 Small, R. J., R. A. Tomas, and F. O. Bryan, 2014b: Storm track response to  
1215 ocean fronts in a global high-resolution climate model. *Clim. Dyn.*, **43**, 805-828.  
1216 <https://doi.org/10.1007/s00382-013-1980-9>.  
1217  
1218 Small, R.J., S.P. deSzoeko, S.-P. Xie, L. O'Neill, H. Seo, Q. Song, P. Cornillon,  
1219 M. Spall, and S. Minobe, 2008: Air-sea interaction over ocean fronts and eddies.  
1220 *Dyn. Atmos. Oceans*, **45**, 274–319.  
1221  
1222 Smirnov, D., M. Newman, M. A. Alexander, Y.-O. Kwon, and C. Frankignoul,  
1223 2015: Investigating the Local Atmospheric Response to a Realistic Shift in the  
1224 Oyashio Sea Surface Temperature Front. *J. Clim.*, **28**, 1126–1147,  
1225 <https://doi.org/10.1175/JCLI-D-14-00285.1>  
1226  
1227 Stephens, G.L., Li, J., Wild, M., Clayson, C.A., Loeb, N., Kato, S., L'Ecuyer, T.,  
1228 Stackhouse, P.W., Lebsock, M., Andrews, T., 2012. An update on Earth's  
1229 energy balance in light of the latest global observations. *Nature Geosci.* **5**, 691–  
1230 696. <https://doi.org/10.1038/ngeo1580>.  
1231



- 1232 Stock, C.A., and Coauthors, 2010: On the use of IPCC-class models to assess  
1233 the impact of climate on living marine resources, *Prog. Oceanog.*, **88**, 1-27,  
1234 <https://doi.org/10.1016/j.pocean.2010.09.001>.  
1235
- 1236 Taylor, C. M., R. A. M. de Jeu, F. Guichard, P. P. Harris, and W. A. Dorigo,  
1237 2012: Afternoon rain more likely over drier soils. *Nature*, **489**, 423-426,  
1238 <https://doi.org/10.1038/nature11377>.  
1239
- 1240 Taylor, K. E., R. J. Stouffer and G. A. Meehl, 2012: An overview of CMIP5 and  
1241 the Experimental Design. *Bull. Am. Meteor. Soc.*, **93**, 485-498,  
1242 <https://doi.org/10.1175/BAMS-D-11-00094.1>.  
1243
- 1244 Terai, C. R., P. M. Caldwell, S. A. Klein, Q. Tang and M. L. Branstetter, 2017:  
1245 The atmospheric hydrologic cycle in the ACME v0.3 model. *Clim. Dyn.*,  
1246 <https://doi.org/10.1007/s00382-017-3803-x>.  
1247
- 1248 Tokinaga, H., Y. Tanimoto, and S.-P. Xie, T. Sampe, H. Tomita, and H.  
1249 Ichikawa, 2009: Ocean frontal effects on the vertical development of clouds  
1250 over the western North Pacific: In situ and satellite observations. *J. Clim.*, **22**,  
1251 4241–4260.  
1252
- 1253 Trenberth, K. E., J. T. Fasullo, and J. Mackaro, 2011. Atmospheric Moisture  
1254 Transports from Ocean to Land and Global Energy Flows in Reanalyses. *J.*  
1255 *Clim.*, **24**, 4907–4924.  
1256
- 1257 Trenberth, K. E., J. T. Fasullo, and J. Kiehl, 2009: Earth's Global Energy  
1258 Budget. *Bull. Amer. Meteor. Soc.*, **90**, 311,  
1259 <https://doi.org/10.1175/2008BAMS2634.1>.  
1260
- 1261 Vellinga, M., M. Roberts, P. L. Vidale, M. S. Mizieliński, M.-E. Demory, R.  
1262 Schiemann, J. Strachan, and C. Bain, 2015: Sahel decadal rainfall variability  
1263 and the role of model horizontal resolution. *Geophys. Res. Lett.*, **42**,  
1264 <https://doi.org/10.1002/2015GL066690>.  
1265

- 1266 Walsh, K., S. Lavender, E. Scoccimarro, and H. Murakami, 2013: Resolution  
1267 dependence of tropical cyclone formation in CMIP3 and finer resolution models.  
1268 *Clim. Dyn.*, **40**, 585–599, <https://doi.org/10.1007/s00382-012-1298-z>.  
1269
- 1270 Walsh K., and Coauthors, 2015: Hurricanes and climate: the U.S. CLIVAR  
1271 working group on hurricanes. *Bull. Amer. Met. Soc.*, **96**, 997–1017,  
1272 <https://doi.org/10.1175/BAMS-D-13-00242.1>.  
1273
- 1274 Walters, D. and Coauthors, 2017: The Met Office Unified Model Global  
1275 Atmosphere 6.0/6.1 and JULES Global Land 6.0/6.1 configurations. *Geosci.*  
1276 *Model Dev.* **10**, 1487-1520, <https://doi.org/10.5194/gmd-10-1487-2017>.  
1277
- 1278 Wang, Q., S. Danilov, D. Sidorenko, R. Timmermann, C. Wekerle, X. Wang,  
1279 T. Jung, and J. Schröter, 2014: The Finite Element Sea ice-Ocean Model  
1280 (FESOM): Formulation of an unstructured-mesh ocean general circulation  
1281 model. *Geosci. Mod. Dev.*, **6**, 3893—3976.  
1282
- 1283 Wang, Q., S. Danilov, and J. Schröter, 2008: Finite element ocean circulation  
1284 model based on triangular prismatic elements, with application in studying the  
1285 effect of topography representation. *J. Geophys. Res.*, **113**, C05015,  
1286 <https://doi.org/10.1029/2007JC004482>.  
1287
- 1288 Watanabe, M., H. Shiogama, Y. Imada, M. Mori, M. Ishii, M., and M. Kimoto,  
1289 2013: Event attribution of the August 2010 Russian heat wave. *SOLA*, **9**, 65-  
1290 68.  
1291
- 1292 Watson, P. A. G., J. Berner, S. Corti, P. Davini, J. von Hardenberg, C.  
1293 Sanchez, A. Weisheimer, and T. N. Palmer, 2017: The impact of stochastic  
1294 physics on tropical rainfall variability in global climate models on daily to weekly  
1295 time scales. *J. Geophys. Res. Atmos.*, **122**, 5738–5762,  
1296 <https://doi.org/10.1002/2016JD026386>.  
1297

- 1298 Wedi, N. P., 2014: Increasing horizontal resolution in numerical weather  
1299 prediction and climate simulations: illusion or panacea? *Phil. Trans. R. Soc. A*,  
1300 372: 20130289. <http://dx.doi.org/10.1098/rsta.2013.0289>  
1301
- 1302 Wehner, M. F., and Coauthors, 2014: The effect of horizontal resolution on  
1303 simulation quality in the Community Atmospheric Model, CAM5.1, *J. Adv.*  
1304 *Model. Earth Syst.*, **6**, 980–997, <https://doi.org/10.1002/2013MS000276>.  
1305
- 1306 Wehner, M. F., Prabhat, K. A. Reed, D. Stone, W. D. Collins, and J. T.  
1307 Bacmeister, 2015: Resolution dependence of future tropical cyclone projections  
1308 of CAM5.1 in the U.S. CLIVAR Hurricane Working Group idealized  
1309 configurations. *J. Clim.*, **28**, 3905–3925, <https://doi.org/10.1175/JCLI-D-14->  
1310 00311.1.  
1311
- 1312 Wild, M., Folini, D., Schär, C., Loeb, N., Dutton, E. G., and König-Langlo, G.,  
1313 2013: The global energy balance from a surface perspective. *Clim. Dyn.*, **40**,  
1314 3107–3134. <https://doi.org/10.1007/s00382-012-1569-8>.  
1315
- 1316 Wild, M., Folini, D., Hakuba, M.Z., Schär, C., Seneviratne, S.I., Kato, S., Rutan,  
1317 D., Ammann, C., Wood, E.F., König-Langlo, G., 2015. The energy balance over  
1318 land and oceans: an assessment based on direct observations and CMIP5  
1319 climate models. *Clim. Dyn.*, **44**, 3393–3429. <https://doi.org/10.1007/s00382->  
1320 014-2430-z.  
1321
- 1322 Williams P.D., 2012: Climatic impacts of stochastic fluctuations in air-sea fluxes.  
1323 *Geophys Res Lett*, **39**, L10705. <https://doi.org/10.1029/2012GL051813>.  
1324
- 1325 Willison, J., W. A. Robinson, and G. M. Lackmann, 2013: The importance of  
1326 resolving mesoscale latent heating in the North Atlantic storm track. *J. Atmos.*  
1327 *Sci.*, **70**, 2234-2250.  
1328
- 1329 Xie, S.-P., 2004: Satellite observations of cool ocean–atmosphere interaction.  
1330 *Bull. Amer. Meteor. Soc.*, **85**, 195–208.  
1331

1332 Yamada, Y., M. Satoh, M. Sugi, C. Kodama, A. T. Noda, M. Nakano, T. Nasuno,  
1333 2017: Response of tropical cyclone activity and structure to global warming in  
1334 a high-resolution global nonhydrostatic model. *J. Clim.*,  
1335 <https://doi.org/10.1175/JCLI-D-17-0068.1>.

1336

1337 Yatagai, A., K. Kamiguchi, O. Arakawa, A. Hamada, N. Yasutomi, and A. Kitoh,  
1338 2012: APHRODITE: Constructing a long-term daily gridded precipitation  
1339 dataset for Asia based on a dense network of rain gauges. *Bull. Amer. Meteor.*  
1340 *Soc.*, **93**, 1401–1415, <https://doi.org/10.1175/BAMS-D-11-00122.1>.

1341

1342 Zappa, G., L. C. Shaffrey, and K. I. Hodges, 2013: The Ability of CMIP5 Models  
1343 to Simulate North Atlantic Extratropical Cyclones. *J. Clim.*, **26**, 5379–5396,  
1344 <https://doi.org/10.1175/JCLI-D-12-00501.1>.

1345

1346 Zarzycki, C. M., M. N. Levy, C. Jablonowski, J. R. Overfelt, M. A. Taylor, and  
1347 P. A. Ullrich, 2014: Aquaplanet experiments using CAM's variable-resolution  
1348 dynamical core. *J. Clim.*, **27**, 5481–5503, <https://doi.org/10.1175/JCLI-D-14-00004.1>.

1350

1351 Zhao, M., I. M. Held, S.-J. Lin, and G. A. Vecchi, 2009: Simulations of global  
1352 hurricane climatology, interannual variability, and response to global warming  
1353 using a 50-km resolution GCM. *J. Clim.*, **22**, 6653–6678,  
1354 <https://doi.org/10.1175/2009JCLI3049.1>.

1355

1356

1357 [Figure captions](#)

1358

1359 Figure 1: Long-term mean precipitation estimates from different sources over  
 1360 the ocean, flat terrain and mountainous terrain (see inset, mountainous area is  
 1361 25% of total land area). Bar chart labels: N96, N216, N512 are 130km, 60km,  
 1362 25km resolution simulations respectively using HadGEM3-GA3 (Mizielinski et  
 1363 al. 2014); N480, “N480, N96 orography” are GA6 (Walters et al. 2016)  
 1364 simulations at 27km resolution, the latter with orography degraded to N96  
 1365 (130km) resolution; N96\*, N216\*, N512\* are the same N96, N216, N512 as  
 1366 above, but with estimates scaled by the global surface net shortwave radiation  
 1367 bias; Observation-based estimates: GPCP (GPCP v2.2, Adler et al. 2012); Wild  
 1368 et al. (2015) (uncertainties not shown); Wild et al. (2013); Stephens et al.  
 1369 (2012); Trenberth et al. (2009).

1370

1371 Figure 2: Comparisons of the annual probability density distributions (y-axis) of  
 1372 daily precipitation ( $\text{mm day}^{-1}$ , x axis) between the models and location specific  
 1373 gridded observations as indicated by the dataset name in parentheses. a:  
 1374 Global land and ocean (GPCP), b: Global land only (UW-Global), c: Tropical  
 1375 land and ocean, 20S-20N (TRMM), d: CONUS (UW-CONUS), e: Asia  
 1376 (APHRODITE), f: Europe (E-OBS). Red, blue, green and black lines  
 1377 respectively represent the  $2^\circ$  CAM5.1,  $1^\circ$  CAM5.1,  $0.25^\circ$  CAM5.1. Observations  
 1378 are represented by the black line in Figure 2a and by gray shading in Figures  
 1379 2b–2f, indicating the range of available data sets. Daily precipitation was  
 1380 remapped onto the  $2^\circ$  grid before computing the distributions in all cases. Any  
 1381 precipitation rates larger than 100 mm/day are assigned to the last bin for  
 1382 normalization purposes that sometimes results in an uptick at the end of the  
 1383 plot. Reproduced from Wehner et al. (2014).

1384

1385 Figure 3: Map showing the lowest best resolution model for each region as  
 1386 defined in the Appendix by comparing daily precipitation histograms.  
 1387 N512=25km, N216=60km, N96=130km mid-latitude resolution. Uncertain  
 1388 implies either no model is clearly better, or that observational uncertainty is too  
 1389 large to determine a best model.

1390

1391 Figure 4: North Atlantic Ocean (left) genesis and (right) track densities as  
1392 number density per season per unit area equivalent to a 5° spherical cap for  
1393 (a), (f) IBTrACS (Obs) and IFS simulations at (b), (g) T2047, (c), (h) T1279, (d),  
1394 (i) T511, and (e), (j) T159 resolutions. Reproduced from Manganello et al.  
1395 (2012) with permission by the authors.

1396

1397 Figure 5: Illustration of comparing Root Mean Square Difference (RMSD)  
1398 values (see Appendix A for details) from models and observations, with  
1399 uncertainty in observations and model ensemble spread both indicated as  
1400 shading, and here RMSD is normalized to one dataset (TRMM in this example).  
1401 One model is clearly best in case a), two models cannot be split in b) due to  
1402 overlap in spread, while in c) the observations disagree too much to assign a  
1403 best model.

1404

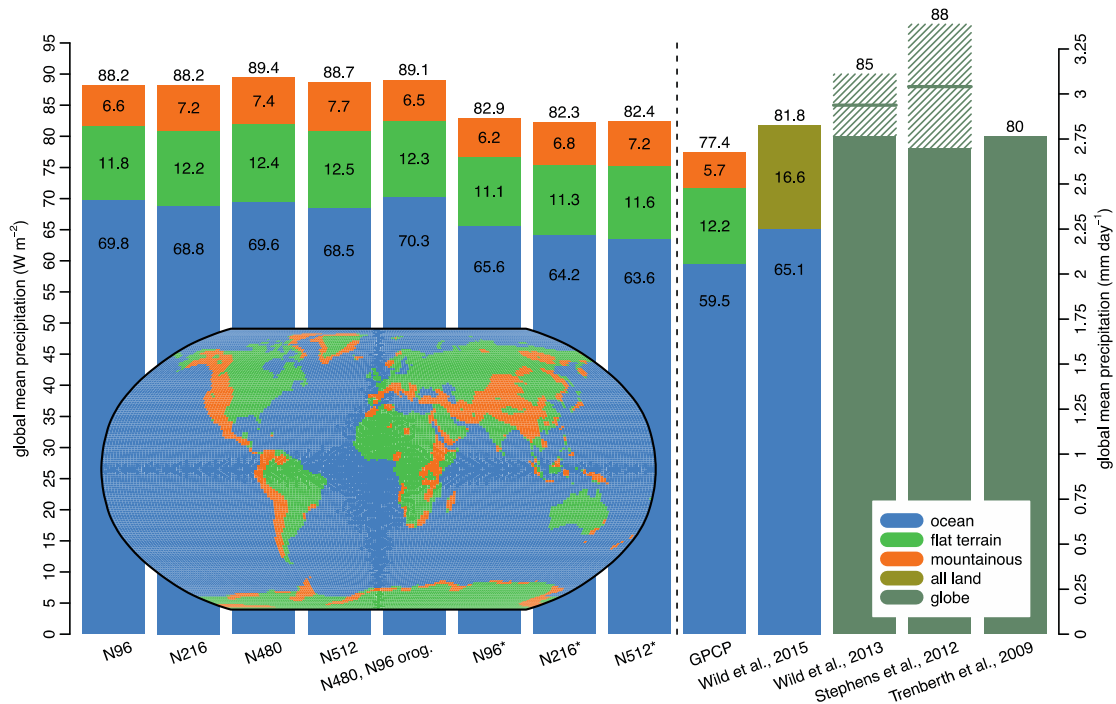
1405

1406

1407

1408

1409



1410

1411

1412 Figure 1: Long-term mean precipitation estimates from different sources over  
 1413 the ocean, flat terrain and mountainous terrain (see inset, mountainous area is  
 1414 25% of total land area). Bar chart labels: N96, N216, N512 are 130km, 60km,  
 1415 25km resolution simulations respectively using HadGEM3-GA3 (Mizielinski et  
 1416 al. 2014); N480, "N480, N96 orography" are GA6 (Walters et al. 2016)  
 1417 simulations at 27km resolution, the latter with orography degraded to N96  
 1418 (130km) resolution; N96\*, N216\*, N512\* are the same N96, N216, N512 as  
 1419 above, but with estimates scaled by the global surface net shortwave radiation  
 1420 bias; Observation-based estimates: GPCP (GPCP v2.2, Adler et al. 2012); Wild  
 1421 et al. (2015) (uncertainties not shown); Wild et al. (2013); Stephens et al.  
 1422 (2012); Trenberth et al. (2009).

1423

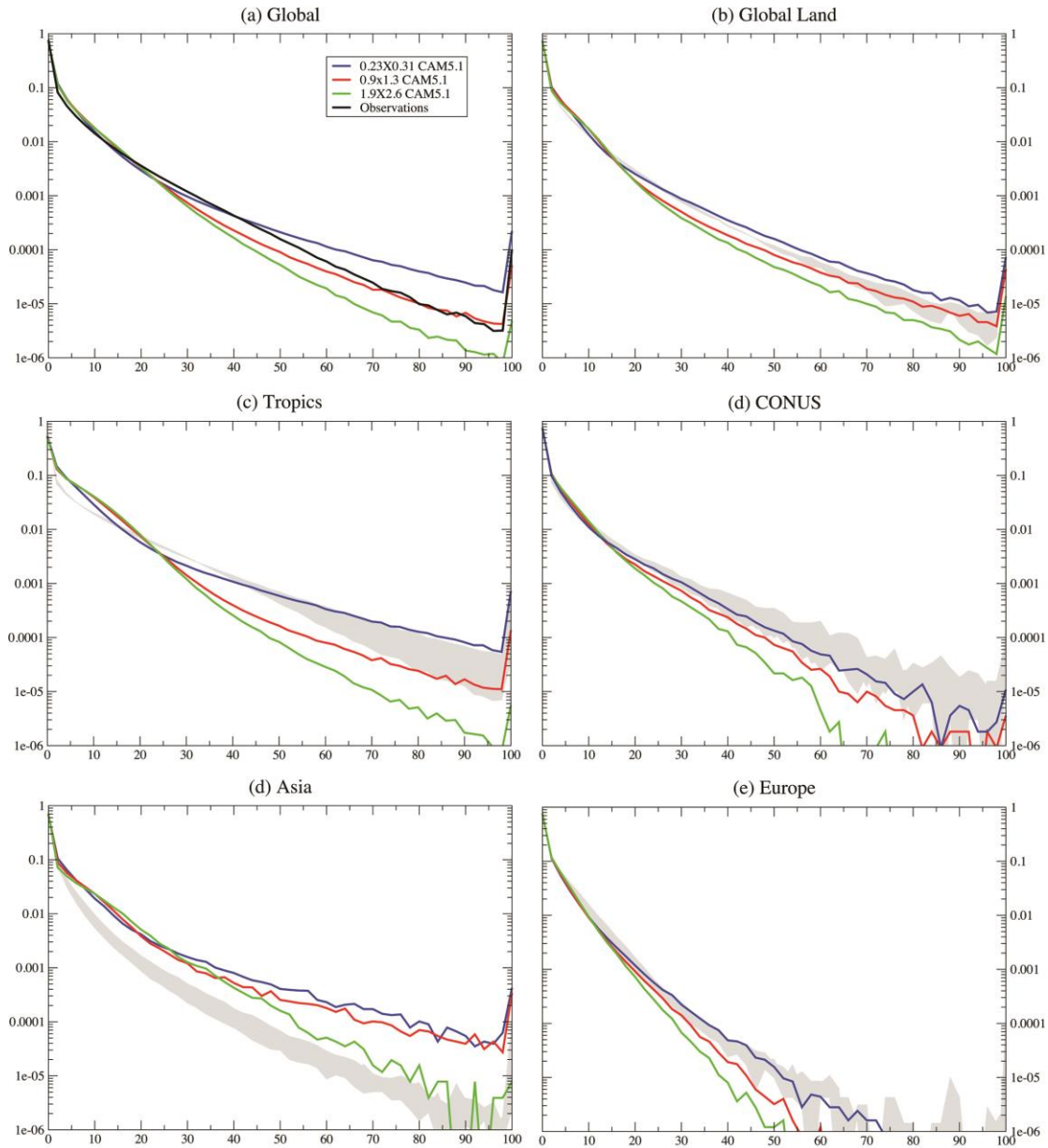
1424

1425

1426

1427

1428



1429

1430

1431 Figure 2: Comparisons of the annual probability density distributions (y-axis) of  
 1432 daily precipitation ( $\text{mm day}^{-1}$ , x axis) between the models and location specific  
 1433 gridded observations as indicated by the dataset name in parentheses. a:  
 1434 Global land and ocean (GPCP), b: Global land only (UW-Global), c: Tropical  
 1435 land and ocean, 20S-20N (TRMM), d: CONUS (UW-CONUS), e: Asia  
 1436 (APHRODITE), f: Europe (E-OBS). Red, blue, green and black lines  
 1437 respectively represent the  $2^\circ$  CAM5.1,  $1^\circ$  CAM5.1,  $0.25^\circ$  CAM5.1. Observations  
 1438 are represented by the black line in Figure 2a and by gray shading in Figures  
 1439 2b–2f, indicating the range of available data sets. Daily precipitation was  
 1440 remapped onto the  $2^\circ$  grid before computing the distributions in all cases. Any



1441 precipitation rates larger than 100 mm/day are assigned to the last bin for  
1442 normalization purposes that sometimes results in an uptick at the end of the  
1443 plot. Reproduced from Wehner et al. (2014).

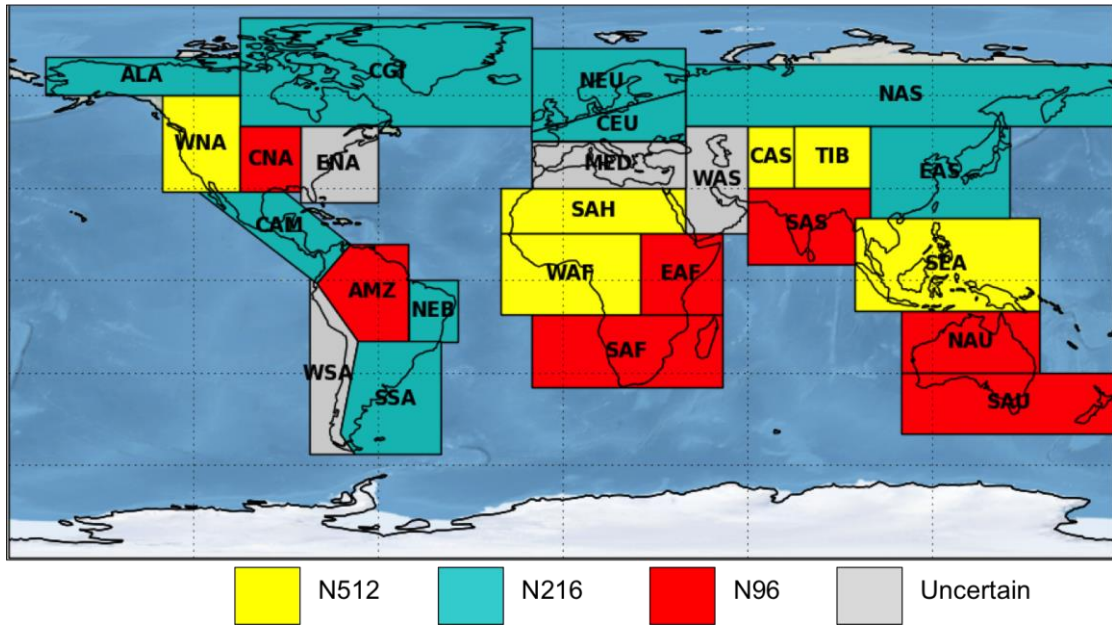
1444

1445

1446

1447

1448



1449

1450

1451 Figure 3: Map showing the coarsest best resolution model for each region as  
 1452 defined in the Appendix by comparing daily precipitation histograms.  
 1453 N512=25km, N216=60km, N96=130km mid-latitude resolution. Uncertain  
 1454 implies either no model is clearly better, or that observational uncertainty is too  
 1455 large to determine a best model.

1456

1457

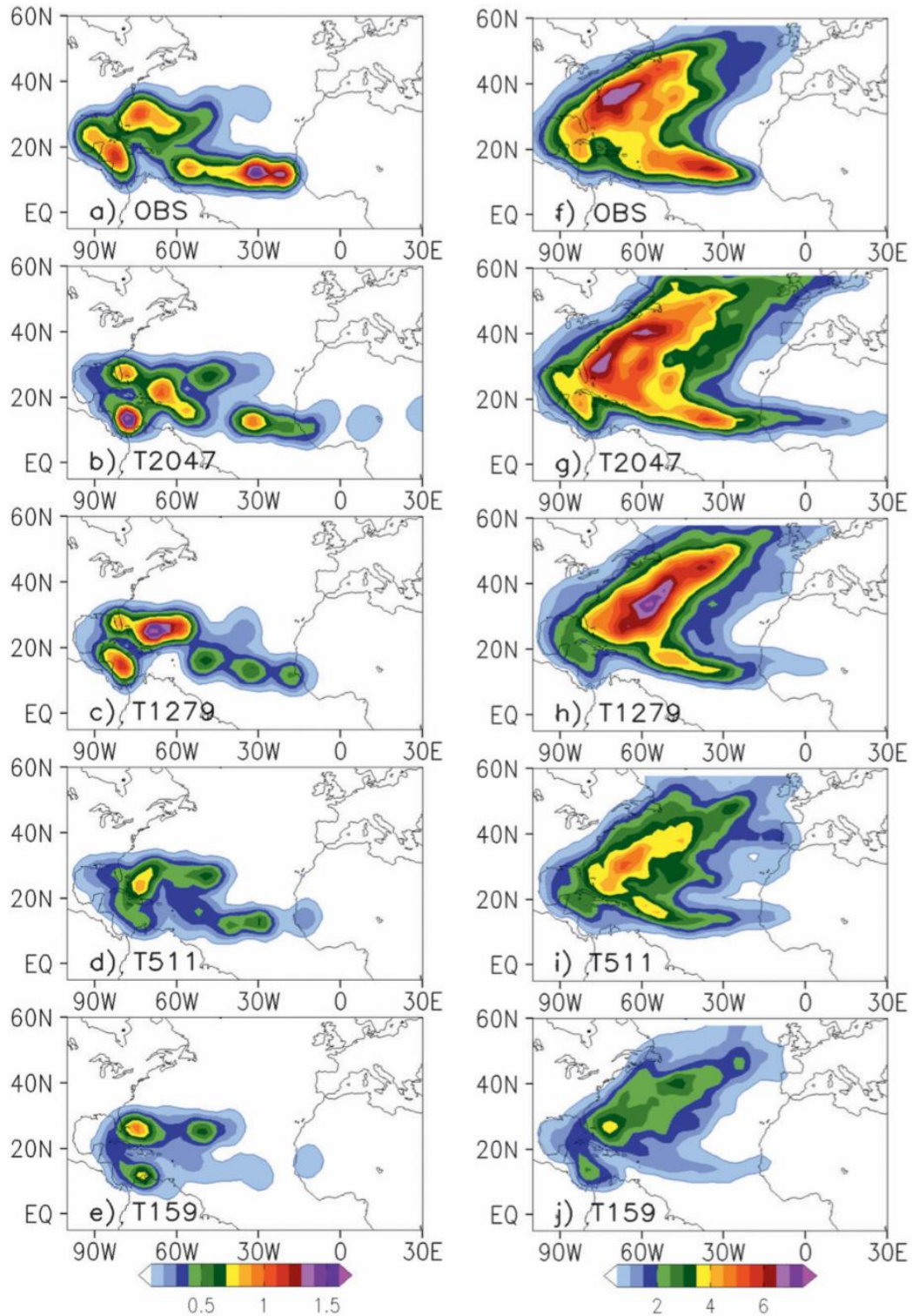
1458

1459

1460

1461

1462

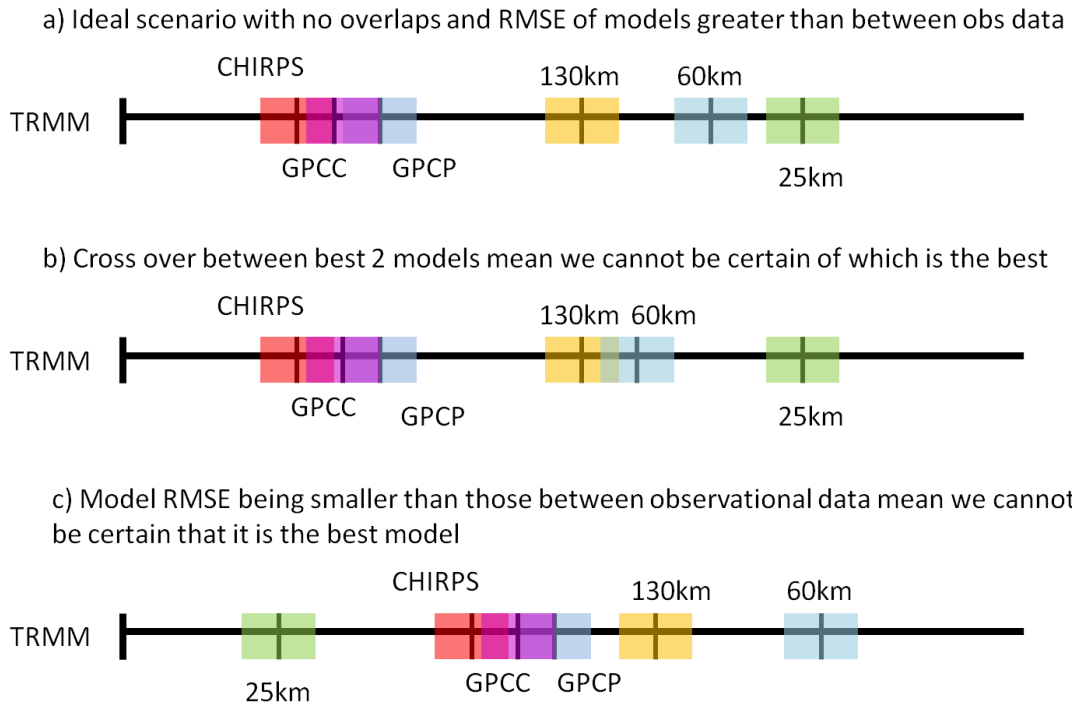


1463

1464 Figure 4: North Atlantic Ocean (left) genesis and (right) track densities as  
 1465 number density per season per unit area equivalent to a 5° spherical cap for  
 1466 (a), (f) IBTrACS (Obs) and IFS simulations at (b), (g) T2047, (c), (h) T1279, (d),  
 1467 (i) T511, and (e), (j) T159 resolutions. Reproduced from Manganello et al.  
 1468 (2012) with permission by the authors.

1469

1470



1471

1472 Figure 5: Illustration of comparing Root Mean Square Difference (RMSD)  
 1473 values (see Appendix A for details) from models and observations, with  
 1474 uncertainty in observations and model ensemble spread both indicated as  
 1475 shading, and here RMSD is normalized to one dataset (TRMM in this example).  
 1476 One model is clearly best in case a), two models cannot be split in b) due to  
 1477 overlap in spread, while in c) the observations disagree too much to assign a  
 1478 best model.